IMPLEMENTATION AND EVALUATION OF NEUROMUSCULAR CONTROLLERS IN ROBOTIC

SYSTEMS PERFORMING COOPERATIVE TASKS WITH HUMANS

By

DANNY GODBOUT

A thesis submitted in partial fulfillment of
The requirements for the degree of

MASTER OF SCIENCE IN MECHANICAL ENGINEERING

WASHINGTON STATE UNIVERSITY
School of Mechanical and Materials Engineering

DECEMBER 2008

To the Faculty of Washington State University:

        The members of the Committee appointed to examine the thesis of DANNY GODBOUT find it satisfactory and recommend that it be accepted.

_____
Chair

_____

_____

IMPLEMENTATION AND EVALUATION OF NEUROMUSCULAR CONTROLLERS IN

ROBOTIC SYSTEMS PERFORMING COOPERATIVE TASKS WITH HUMANS

Abstract

By Danny Godbout, M.Sc.
Washington State University
December 2008

Chair: David Lin

To date, the majority of research on Human-Robot interaction (HRI) has focused on the appearance and cognitive abilities of robots. This has led to the research and development of anthropomorphic, collaborative, gesture recognizing, and social robots behaving and interacting in humanoid fashion to improve HRI. However, this concept has not been extended to robots that physically *feel* like a human as was explored in this study.

A neuromuscular controller was implemented in a robot performing a cooperative postural task with a human. The performance of the human in collaboration with the human-like robot was hypothesized to improve when compared to the performance of the human with the same robot controlled via a standard proportional-derivative (PD) controller by presenting a more intuitive interface.

Team performance was tested with static and dynamic postural tasks designed to limit participation to intrinsic muscle and spinal reflex responses. The experimental setup demanded that the team support a load in a neutral position with both operators supported at the elbow and holding their forearms vertically. The static task evaluated the ability of the team to hold the load in the neutral position over a 30 second period, and the dynamic test observed the performance

of the team returning to the neutral position after subjecting the load to an 8 Nm, 35 ms perturbation.

Results of the static trial were significant (p=0.048) for the root mean squared (RMS) displacement metric, signifying less sway with the PD model when holding a posture. Dynamic test results, by contrast, showed significantly (p<0.01) improved performance with the human-like model for reducing the peak displacement of the load following a perturbation. The static performance measure of peak displacement, and the dynamic measures of settling time and settling error showed no statistically significant (p=0.05) differences between models.

The results observed are in line with previously observed characteristics of human impedance as a compliant, heavily damped system. The human-like robot complimented these characteristics to provide a combined team performance that, while more compliant and therefore less accurate, is more robust to dynamic perturbations as would be experienced in uncontrolled environments.

TABLE OF CONTENTS

LIST OF FIGURES

LIST OF TABLES

CHAPTER ONE

INTRODUCTION

While the fields of artificial intelligence, automation, and industrial robotics have been explored for decades, robots have only recently begun the transition from research and industrial environments into our daily lives. In a 2006 Scientific American article [Gates; 2006], Bill Gates described the robotics industry as primed for expansion out of commercial use and into domestic applications in the same way the PC industry was in 1970. As robots enter daily life, the controlled environments they were once designed for are no longer taken for granted- a typical home or work environment is a dynamic one that requires rich interaction with both living and non-living factors.

Much of the research undertaken to advance the state of the art in interactive robotics has focused on the behavioral abilities of robots. Robots being complex, non-living entities, cause humans to resort to established social models to understand and predict the behaviors of the robotic operators [Reeves & Nass; 1996]. As all humans employ some form of social interaction in their daily lives, little training is necessary to communicate and cooperate effectively with a robot making use of social models [Breazeal; 2003]. As robots begin to proliferate into the daily lives of the general population, it becomes increasingly important to ensure that robots conform to the social models engrained in the people they will interface with.

Socially adept robots deliver a platform with which humans can effectively communicate orally and visually, but do not address the quality of physical interaction

between humans and robots. Numerous tasks encountered in a daily routine require the physical cooperation of two or more operators, such as shaking hands, carrying heavy or awkward loads, exchanging objects, and performing complex maintenance tasks. These cooperative tasks are often performed without communication to synchronize strategies between the operators, and require subtle modulation of forces to match both loads and other operators [Reed et. al.; 2004].

This study investigates the implementation of robotic control systems based on human neuromusculoskeletal models as a means of simulating human-like characteristics to improve the quality of human-robot interaction. Similar to the concept that humans communicate most effectively when they can make use of social models, the underlying premise of this research is:

Robots exhibiting human-like mechanical properties will allow human operators
to rely on long-mastered skills of physical interaction with humans.

More specifically, by evaluating the performance of a human-robot team during a common postural task, the characteristics of human-like and traditional control models can be compared in the context of cooperative performance. From the standpoint of mechanical impedances, the dynamic forces of systems generated by motion [Hogan; 1991], it is hypothesized that the impedance of the robot could affect the impedance produced of the human in a cooperative task by affecting kinematic variables such as frequency or amplitude of motion.

As a foundation for understanding physical human-robot interaction, this study will evaluate a postural task that is not subject to voluntary intervention, the conscious, strategic manipulation of muscle activation to adjust limb impedance. Voluntary interaction may provide a greater potential for differentiation between anthropomorphic and standard controllers because the human operator often adapts to the robot (*i.e.,* motor learning). An anthropomorphic controller could provide a more familiar, intuitive mechanical interface for this type of interaction. While voluntary movements may ultimately contain the most valuable information, it is crucial to first evaluate and understand the underlying intrinsic and reflex properties of human operators interfacing with robots during a postural task before adding the layer of voluntary control.

CHAPTER TWO

BACKGROUND AND SIGNIFICANCE

2.1 Human-Robot Interaction:

The field of human-robot interaction (HRI) concerns itself specifically with optimizing interfaces between humans and robots. The HRI field was birthed from hazardous materials handling where a need existed for the ability to tele-operate a robotic operator safely and effectively [Adams; 2005A]. Because of this history, much of the work in HRI is concerned with handling instructions and management of multiple tasks. As robots become more intelligent, and therefore more autonomous, human users are able to spend less time instructing single robots, creating free time that can be used productively by instructing teams of robots. As the number of operators increases, the need for effective HRI interfaces becomes key to limiting errors resulting from neglect [Crandall; 2005], physical limitations [Trafton; 2005], or simply from human error.

While research exploring the industrial applications of HRI is very active, the presence of more inexpensive, varied, and effective embedded systems and actuators have seen robotics enter the daily lives of humans as appliances, toys, and aids for the elderly among other applications [Breazeal; 2003]. With the hopes of creating robots that are a constructive part of humans' daily lives, HRI is growing to encompass the development of humanoid robotics. Operating on the principle that humans are already experts in social interaction [Breazeal; 2003], a common theme has manifested stating that human-human interaction should be followed as a model for human-robot interaction [Trafton; 2005]. An interface will be ineffective for most users if it does not conform to

norms of human perception and interpretation. This theme has driven research in social robotics to exploit human characteristics as a means of improving communication and collaboration. This branch of research includes the exploration of a variety of behavioral characteristics and their effect on HRI, including humanoid learning [Breazeal; 2003], physical appearance and gestures [Minato; 2004], cooperative communication [Trafton; 2005], expressiveness and attention [Bruce; 2002], and even such subtle cues as gaze patterns during conversation [Sidner; 2004].

Despite the expansion in the field of HRI, little research exists that explores physical, cooperative interaction between humans and robots. Some work has recognized the proliferation of robots into humans' daily lives as an impetus to improve tactile interfaces [Wosch; 2002], but no research has been found on the use of humanoid control models as a means of improving HRI. The environments within which humans work are often designed for human morphology, for example ergonomic or human factors design [Norman; 2002]. Redesigning environments or training humans to interact with robots using novel (to a typical user) mechanical properties may is a limited and ineffective way to introduce robots to mainstream applications [Breazeal; 2003]. The hypothesis of this research is that robots simulating anthropomorphic mechanical properties could potentially integrate with humans more easily by conforming to expected mechanical behaviors. The predictability and familiarity of anthropomorphic properties may reduce the learning curve required for humans to cooperate effectively with the robotic operator as the human can exploit well-known control schemes instead of adapting to a new type of load, similar to socially adept robots that have improved human-robot interfaces by

5

capitalizing on long mastered skills [Breazeal; 2003]. Furthermore, emulating properties that have proven to promote robust and dexterous control in humans could improve the performance of a robot in uncontrolled, complex environments. While studies have explored the development of anthropomorphic actuators and their effects on robotic performance [Klute et. al.; 2002], none have evaluated how the anthropomorphic properties of the actuators affected HRI as this study does.

2.2 Cooperative Tasks and Human Impedances

Typical interaction between humans occurs in many ways with varied expectations. This study is most concerned with cooperative tasks between operators, that is:

Two or more operators performing a goal-oriented task requiring coupled contributions from all operators.

Cooperative postural tasks, a team-lift for example, are ideal for this study as they require input from all operators, and inputs from one operator will directly affect the other operator. Postural tasks involving humans have been studied extensively [Chiari, 2000; Mussa-Ivaldi, 1985; Zhang and Rymer, 1997; Lan, 1995; Collins and DeLuca, 1995] and therefore provide a more thorough understanding of the factors affecting the outcomes of the task. As human participation during postural tasks can be limited to non-voluntary action [Ganong; 2005], variability between and within subjects is reduced and

biological control models implemented in the robot can be designed and tested with higher fidelity.

Previous studies of human-human cooperative tasks have shown that even when two teammates cannot communicate through verbal or visual cues, interaction still occurs through the touch-based physical link that connects them. For example, a study was conducted in which two operators could not see or speak to each other and acted on opposite ends of a rotating beam to place it in a target position [Reed; 2004]. The results showed physical interaction through specialization. When specialization occurred, the operators acted with opposing antagonist forces to control the overall motion. This results in shorter times to arrive at the target as compared to single operator movements. The current study seeks to investigate this interaction of mechanical impedances when the operators are a human and a robot. Mechanical impedance, in the context of this study, is defined as:

"Mechanical Impedance is a dynamic operator which specifies the forces an object generates in response to motions." [Hogan; 1991]

The interaction of mechanical impedances is important because it has been shown that human mechanical impedance is operating range dependent. One example of this is the stretch reflex, the modulation of skeletal muscle force under the control of spinal reflexes in response to lengthening. When a muscle is stretched, the muscle spindle (a sensory organ) increases its afferent firing rate and directly increases the activation of the

same muscle's motoneuron. This feedback mechanism produces more force to counteract the disturbance [Ganong; 2005]. In humans, the stretch reflex has been shown to be amplitude and frequency dependent, such that its impedance properties are affected by the characteristics of the motions encountered in a postural task. Amplitude dependent characteristics of the interphalangeal joint of the thumb were evaluated with varying inertial loads and perturbation sizes [Lin, Rymer; 2001]. Results showed that as displacement and velocity amplitude of the perturbation increased, the damping of the joint also increased, providing evidence of non-linear damping properties in human muscle. The frequency dependent properties show that viscous damping decreases with increasing frequency for low frequencies, and negative viscosities can occur between 7 to 11 Hz at the elbow for displacements less than approximately 1 cm at the wrist [Joyce et. al.; 1974]. A less-stiff robotic controller tuned for a lower natural frequency could therefore optimize the performance of the human operator by shifting their performance towards a more heavily damped state. A slightly less-stiff controller would also increase the initial transient amplitude, potentially resulting in a more damped response from the human subject.

2.3 Standards in Robotic Control:

The proportional-integral-derivative (PID) control algorithm is a popular control method for engineered systems [Guttirez; 2007], and was thus chosen as the "standard" controller for this study. A typical PID controller operates on the basis of a set point. The set point is subtracted from the current output state to produce an error signal (Figure 2.1). This error signal is then fed through three gain loops that are then summed to

produce output acting on the plant, such as the torque in the case a motor used in a robot. The three gain loops are:

- P: The proportional gain produces a torque that is directly proportional to the error signal. A low proportional gain will result in a soft controller, while a high proportional gain may result in instability and oscillation.

- I: The integral gain produces a torque by integrating and scaling the error over time to reduce steady state settling error that can be caused by gravity or friction. Low integral gains have a slow steady-state settling effect; while aggressive integral gains cause overshoot because negative errors must be integrated away by positive error to settle.

- D: The derivative gain produces a torque proportional to the derivative of the input, effectively damping the output of the model. Derivative gain has the advantage of reducing overshoot and oscillation, but large derivative gains are sensitive to noise amplification when the error signal is differentiated.
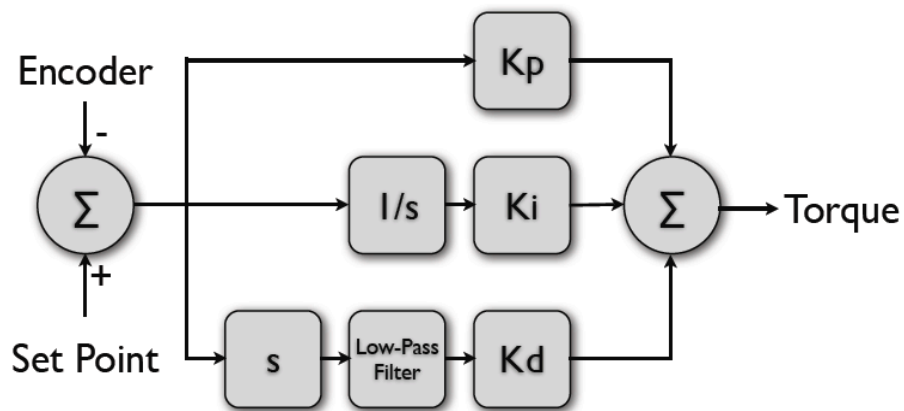
Figure 2.1: Typical PID configuration. *Kp*= Proportional Gain; *Ki*= Integral Gain; *Kd*= Derivative Gain.

The overall mechanical impedance of the PID controller is then a force consisting of proportional, integral, and derivative contributions obtained from the feedback loop.

Knowing the effects of each loop gain, the PID controller can be "tuned" by adjusting the proportional, integral, and derivative gains to achieve the desired response. The PID model is popular in large part because of the ease with which it can be implemented [Guttirez; 2007]. The PID controller can be tuned by feel, analytical methods [O'Dwyer; 2006] or standardized tuning methods including the Cohen-Coon and Ziegler-Nichols techniques [Rivera et. al.; 1986]. Because of the wide range of applications, P, PI, PD, and PID controllers have seen implementation in a variety of fields, including robotics [Guttirez; 2007].

Notably, expansion on PID control schemes has explored techniques that approximate the fundamental properties of human neuromuscular systems. Basic models represent the human neuromuscular system as a viscoelastic element, a proportional spring element in parallel with a damper, effectively a PD controller [Bronzino; 2006]. More detailed models of the neuromuscular system reveal that the viscoelastic characteristics are actually non-linear [Hill; 1938]. Robots performing tracking movements have been shown to improve performance when making use of non-linear PD (i.e. non-linear viscoelastic) control models that adjust the proportional and derivative gains as a function of the error signal [Ouyang, Zhang, 2002; Su et. al., 2004].

2.4 Biological Control

Performance of a postural task is driven by the mechanical impedance of the participating limbs, which can be experimentally measured in the absence of voluntary intervention [Perreault et. al.; 2000]. The maintenance of posture without voluntary intervention is not open loop; spinal feedback mechanisms are still employed to maintain posture. The dynamic stiffness parameters can be artificially separated for analysis into two major components [Kearny et. al.; 1997] acting through the muscle as diagramed in Figure 2.2:

- Reflex Stiffness: Position and velocity sensitive stiffness resulting from the modulation of muscle activation by the stretch reflex.

- Intrinsic Stiffness: Passive viscoelastic and inertial properties of the joint and limb, and the non-linear viscoelastic properties of the active muscle.
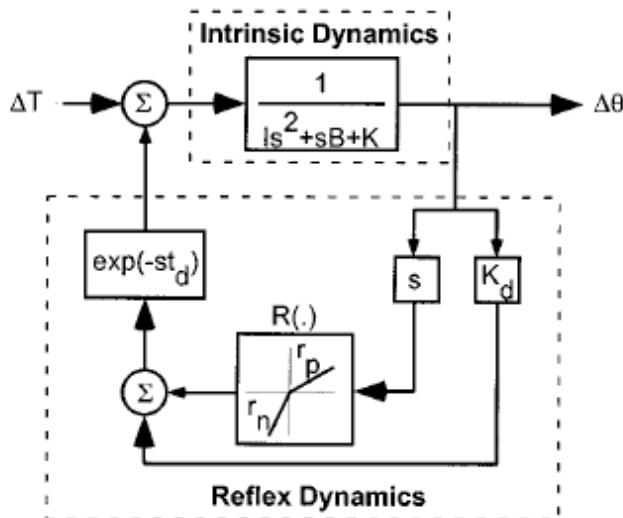
Figure 2.2: Separation of intrinsic and reflexive parameters affecting dynamic stiffness. [Perrault et. al., 2000].

Because the stretch reflex is a monosynaptic reflex, it produces in a relatively fast increase in force that is not subject to the delays of voluntary interventions. Stretch reflex delays in the *biceps brachii* are on the order of tens of milliseconds [Perrault, Crago, Kirsch; 2000]. The muscle spindle response is directionally dependent, specifically a dynamic response that is more sensitive to lengthening than shortening [Perrault et. al.; 2000]

The intrinsic (i.e., non-reflexive) viscoelasticity of the limb arises primarily from joint and muscle properties during constant activation. Passive elastic properties of a joint are generally small over the majority of the functional range of a limb, and increase rapidly as the limits of the range of motion are approached [Winters; 1985] (dotted passive trace in figure 2.3). The peak isometric (i.e., static) force of the active muscle, conversely, crests at an optimal operating point and decreases as the joint rotates away from the optimal point (figure 2.3).
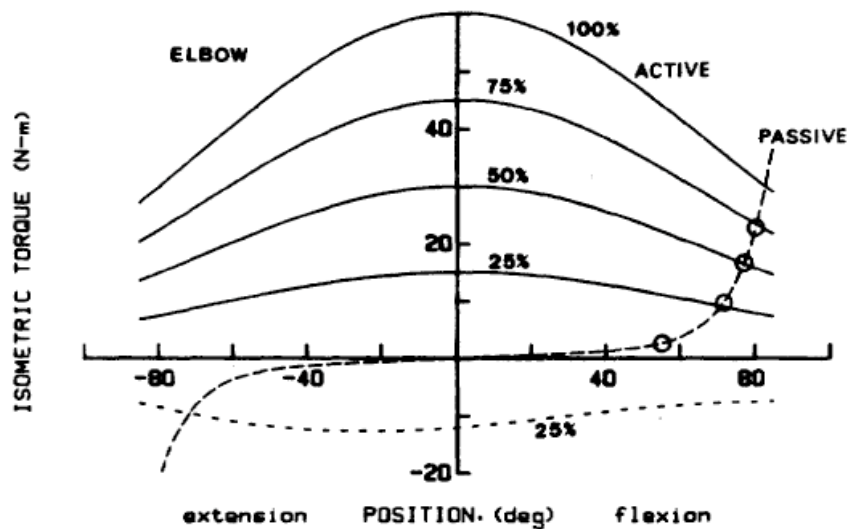
Figure 2.3: Schematic representation of elbow active (solid) and passive (dashed) elastic forces (Winters, 1985).

Active muscle displays non-linear viscous properties, which are described by its force-velocity properties. Namely, muscle force decreases during shortening and increases during lengthening in a hyperbolic manner [Winters; 1985] (shown schematically in figure 2.4).
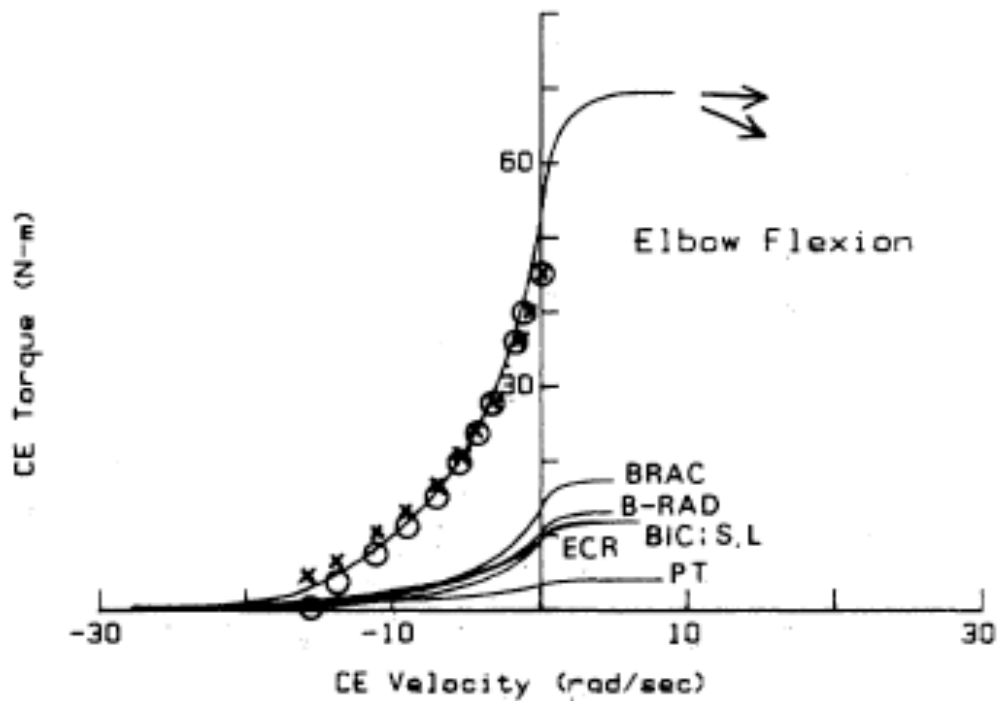
Figure 2.4: Schematic of torque-velocity properties for the elbow contractile element (CE). Bottom curves represent individual elbow flexors, top curve represents the combined contributions of the flexors [Winters, 1985].

A commonly used model representing the non-linear viscoelastic properties of human muscle is the Hill model. The Hill muscle model describes the muscle as a non-linear elastic element, referred to as the series element, in series with a parallel combination of a force producing contractile element, elastic element, and viscous element [Feng; 1998] (Figure 2.5). This model is commonly used for both its fidelity to

13

human muscle, and the fact that the Hill parameters have clearly relevant meanings such as maximum velocity and curve concavity [Winters; 1985].
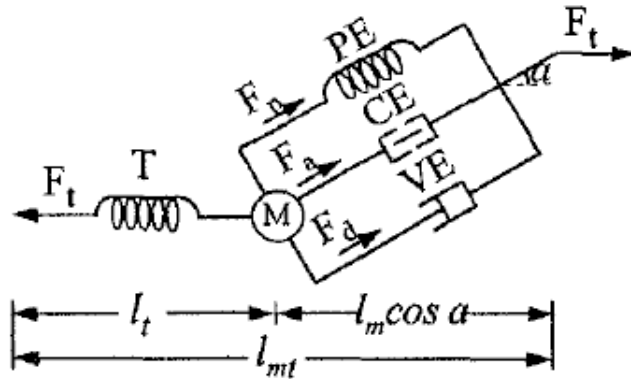
Figure 2.5: Hill muscle model. [Feng, 1998] T= Tendon; PE= Parallel elastic element; CE= Contractile element; VE= Viscous element; M= Muscle mass; F_p= Passive force; F_a= Active contractile element force; F_d= Damping element force; F_t= Muscle force; L_t = Tendon length; L_m = Muscle length; L_{mt} = Muscle and tendon length; α= Pennation angle of muscle fibers.

Variations on the Hill model have adjusted the lengthening behavior to better match measured performance [Close; 1972], include skeletal geometry to define torques in terms of joint angles [Wilkie; 1950], and lumped the agonist and antagonist muscles for a given joint [Winters; 1985].

RESEARCH QUESTION

Extensive research in HRI has been performed within the context of visual, auditory, and behavioral interactions, leaving a valuable aspect of common interaction yet to be explored: physical interaction. This study aims to introduce physical interaction to the body of HRI research, aiding in the development of robots that can be effectively deployed into homes, workplaces, and other uncontrolled environments with untrained operators. Of specific importance are:

- Cooperative task: the task should simulate a commonly performed cooperative task as a direct, relevant indicator of performance in tasks where aide robots may be employed.
- Anthropomorphic control: following the successful implementation of anthropomorphic properties in HRI, it is believed that a human-like controller may improve physical interaction by providing a physical interface that is more closely matched to the mechanical impedances of typical humans.

Two aspects of a postural task were evaluated during this study to understand the benefits and drawbacks of anthropomorphic controllers. A "static" analysis measured the ability of the human-robot team to maintain a constant posture without being subjected to any disturbances, while a "dynamic" analysis measured the response to perturbations applied during the maintenance of posture. A standard control algorithm was used in

identical tasks to provide performance benchmarks against which the human-like control scheme was compared.

The design of the study produced three series of hypotheses addressing the static performance, dynamic performance, and consistency of the dynamic performance for the two control algorithms by examining disturbance rejection and steady-state variables during a cooperative, gravitational holding task. It was hypothesized that an anthropomorphic robotic control model would improve the performance of the human-robot team in these areas by providing a mechanical impedance interface that is better matched to the physical properties of human subjects, that is one that better meets the expectations and natural behaviors of the human operator during such tasks.

CHAPTER FOUR

METHODS

4.1 Postural Task Overview

With the defined purpose of evaluating the effects of anthropomorphic robotic control on human-robot interaction, a protocol was developed to simulate a commonly performed cooperative task. The task chosen was a variation of a team-lift, one example of which could be two operators carrying a table. This was a task chosen for its relative simplicity (no training is required for participation) and the fact that it is a postural task that relies more heavily on reflex response and less on verbal communication and volitional strategy between operators. Subjecting them to a perturbation and evaluating their ability to maintain posture after the perturbation onset also tested the disturbance rejection properties of the human-robot team.

Though the simplicity of carrying a table is taken for granted when performed, it is a task comprised of complex kinematic operations employing many mechanical degrees of freedom by all operators. The voluntary intervention of the operators adds another layer of complexity to the task [Boyd; 2000] as each subject may make use of different control strategies. In order to reliably identify and control the variables affecting each trial, it was necessary to constrain the task to a simpler model with one degree of freedom. It was assumed that when lifting a table the hand-table coupling behaved like a pin-joint, wrist was fixed, and the shoulder acted passively to allow translation of the elbow joint, resulting in a two-degree of freedom system (Figure 4.1) with torque provided by the elbow joint only.
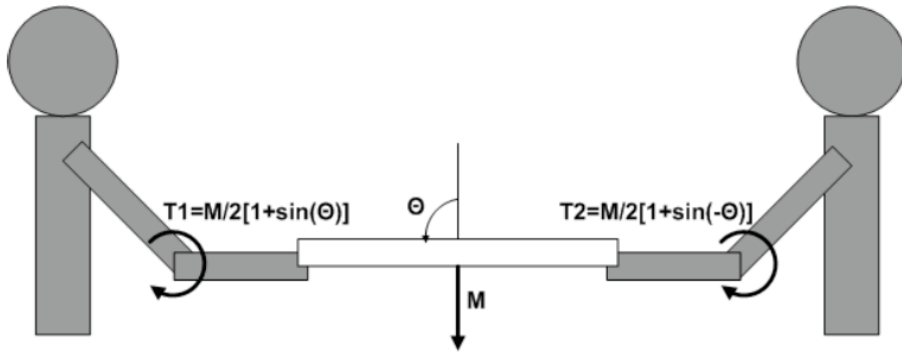
Figure 4.1: Table lifting task illustration. M= mass of load, Θ= board angle.

The system was further constrained to a single degree of freedom implementation by seating the human subject in a chair, resting their upper arm on a stationary wedge form, and splinting the wrist to isolate all torque contributions to the elbow joint (Figure 4.2). The robotic operator was constrained to the "elbow" joint, and one passive "hand" joint secured to the board.
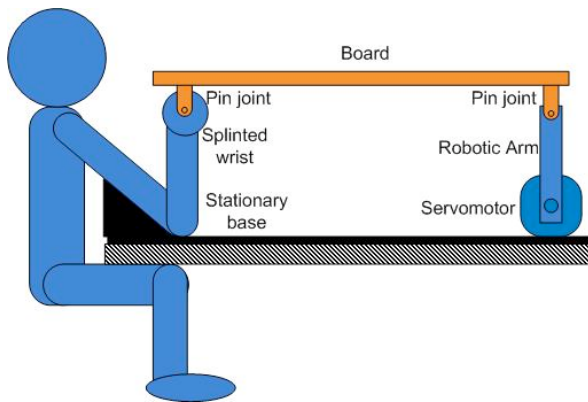
Figure 4.2: Single degree of freedom task implementation.

Constraining the kinematics of the task to one degree of freedom provided two significant benefits. First, it allowed for the isolation of a single torque-producing joint. This was significant in that it reduced inter-subject variability due to differences in muscle activation of different muscles. Where an unconstrained task would allow

different relative levels of contribution from the joints of the legs and arms, the constrained task limited all torque control to the elbow joint. A single degree of freedom was also advantageous in that it directly coupled the robot and human operators. With the freedom afforded by the multiple degrees of freedom in a team lift, the movements of one operator within a reasonable range could have little effect on the other operator outside of some small fluctuations in load distribution. For example, if a team is told to hold a table six inches above the ground and one operator leaves the table on the ground, the other operator can still lift their end of the table to six inches. In a single degree of freedom system the two operators are directly coupled, meaning that the actions of each operator directly impact the other. This was beneficial for this study as it allowed for the evaluation of the direct interface between human and robot without decoupling imposed by a load.

The single degree of freedom implementation described did have some shortcomings inherent to directly coupling the two operators. With both operators' forearms in a vertical position, there was no load torque presented to either operator as when lifting a mass against gravity (Figure 4.1). Furthermore one operator could allow the other to perform the task entirely without penalty. For example the human could behave completely passively and obligate the robot to correct the perturbation alone. In figure 4.1, we see that if one operator does not participate satisfactorily, the board will tilt in their direction, shifting the mass in their direction and ultimately causing the team to fail the task. Because the single degree of freedom task used in this study (Figure 4.2) did not penalize for a lack of participation, it was necessary to create a "virtual load" to

19

simulate the loading of constant gravity and contribution penalties incurred with a natural cooperative task (Figure 4.3).
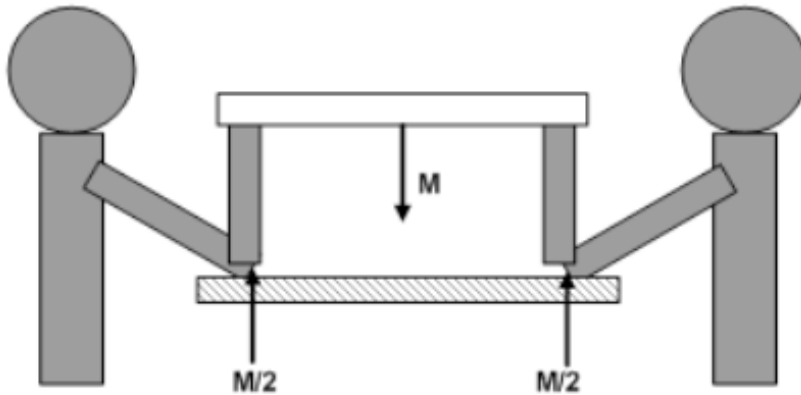
Figure 4.3: Single degree of freedom task forces at equilibrium.

The primary function of the virtual load was to simulate the mass of an object being carried. In this implementation, the motor produced a 2.5 Nm torque in flexion to simulate the weight of an object (clockwise rotation in figure 4.2). With this configuration, both operators were producing 2.5 Nm in flexion at equilibrium, similar to a constraint where operators would be producing force in flexion at the elbow when carrying a table. This bias load carries the additional benefit of isolating the contribution of the human subject to only elbow flexion (as verified by electromyography (EMG) measurement in this study, see section 4.5.1). Controlling co-contraction further reduced the complexity and variability of the human system by preventing force strategies relying on varying levels of co-contraction of elbow flexors and extensors.

The virtual load applied through the motor also simulated the penalties resulting from inadequate performance in the cooperative lifting task. When one operator supports their end of a load lower than the co-operator, they must support a greater relative portion of the mass of the object. Incorporating the 2.5 Nm of bias torque produced to support the object, the mass distribution equation was:

$$T = 2.5(1 + \sin(\theta_L))$$
Eq. 4.1

where T is the torque supported by the human operator and θ_L is the angle of the load. Because of the implementation of the task, the two operators were always operating inversely from each other, that is when the human was "too low" (elbow extended), the robot was "too high" (elbow flexed) and vice-versa. This made the angle of the virtual load, θ_L, directly proportional to the angle of the human subject's arm.

$$\theta_L = L\theta_H$$
Eq. 4.2

where θ_H is the angle of the human subject's arm and L is a scaling factor based on the ratio of the length of the human arm to the length of the board. Defining the vertical positioning of the forearm as 0°, flexion as negative, and extension as positive, the torque supported by the human reduces towards zero as the human flexes towards -90° and increases towards 5 Nm as the human extends towards 90°. Due to the single degree of freedom implementation of the task, a torque penalty on one operator reduced the load on the other operator (as expected in observance of the conservation of mass).

During dynamic trials the board was subjected to an 8 Nm, 35 ms torque pulse, chosen experimentally to produce detectable displacement while staying within the torque producing capabilities of the hardware, and remaining small enough not to cause a variable startle response [Eaton; 1984]. The perturbation disturbed the position of the load and required the human-robot team to return to equilibrium. The perturbation was also applied through the torque motor and occurred at a random time during the trial.

4.2 Robotic Implementation

4.2.1 Mechatronic Design:

The robotic operator was designed to simulate the hand pin joint and elbow of a human arm, with torque being produced exclusively by the elbow via a DC servomotor. The mechanical arm was directly coupled to a 33" board via wood screws on each "hand" (Figure 4.4).
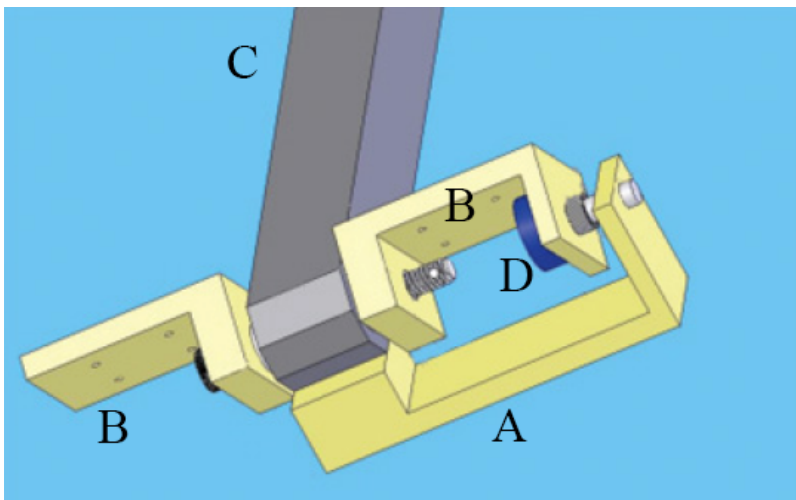
Figure 4.4: Hand configuration on mechanical arm. The dark grey beam represents the mechanical arm. Note the holes drilled in each of the two hands for attachment to a load. A: Potentiometer shaft mount. B: Hand with attachment points for board. C: Robotic arm, coupled to servomotor. D: Potentiometer.

Each hand (Figure 4.4B) was secured to the arm by a single shoulder bolt passing through the arm (Figure 4.4). ABEC-3 type bearings at the interface between the shoulder bolt and mechanical arm ensured smooth, low-friction rotation of the hands. Finally, a 2.5 kΩ potentiometer with a 250° range (3852 cermet-type linear potentiometer, Bourns Inc., Riverside, CA.) was attached to one hand (Figure 4.4-D). The shaft of the potentiometer was coupled to an extension (Figure 4.4-A) attached directly to the arm. In this configuration, the voltage measured across the potentiometer was directly proportional to the angle between the arm and hand attached to the board. The output of the potentiometer was filtered with a second order (-40 dB/dec) Sallen-Key low-pass active filtering circuit tuned for a cutoff frequency of 24 Hz and a Q-factor of 0.732. The 24 Hz cut-off frequency was specified approximately one decade higher than the maximum expected frequency content of 2 Hz, determined experimentally through preliminary perturbation trials. The filter Q-factor of 0.732 was tuned to be close to an ideal value of $1/\sqrt{2}$, ensuring a critically damped response from the filter, maximizing stop-band attenuation while minimizing ripple near the cut-off frequency.

The mechanical arm was constructed with 6061 alloy 1.5" square aluminum tubing with 1/8" wall thickness. The arm measured 12" from the center of the motor shaft to the center of the shaft connecting the hands, approximating the length of an average human forearm [Clauser et. al.; 1969].

A DC servomotor (AKM53G-ANCNR DC Brushless Servomotor; Danaher Motion; Radford, VA.) driven by a servo drive (Kollmorgen Servostar 606 Amplifier;

Danaher Motion; Radford, VA.) produced the torque for the mechanical arm. The DC motor implemented analog resolver feedback that was converted to a simulated 4096 lines/revolution quadrature encoder by the drive. The encoder and wrist potentiometer feedback signals were communicated to a PC using a digital signal processing (DSP) board (dSpace DS1103 board, ControlDesk 4.2 software; dSpace GmbH; Paderborn, Germany) sampling at 1 kHz. Feedback signals were utilized in the controller algorithms programmed in MATLAB/Simulink (The Mathworks; Natick, MA.). Software compiled C code from the Simulink diagrams to control the embedded hardware in the DSP board. The board performed the digital to analog conversion on the control algorithm outputs to communicate the torque output to the Kollmorgen servo drive in force control mode.

Safety systems were implemented via hardware and software position sensors, a manual kill switch, and software velocity sensors that all disconnected mains power to the motor in case of motor run-off. Mechanical stops prevented the arm from rotating outside of the designated range.

4.2.2 Software Design:

Two control models were chosen for implementation in the static and dynamic trials. One model was to represent a standard control scheme that could likely be encountered in existing robotic operators. The second model was designed to simulate the neuromuscular properties of the human elbow acting in flexion to match the operating conditions of the human subject. A list of criteria was established to structure the model

selection process. The selection criteria are listed in table 4.1. Cells labeled with an "X" indicate a criterion that applied to the respective model.

Table 4.1: Model selection criteria.

Criteria	Human-like model	Industry-standard model
1. Remain stable after the onset of a perturbation to promote safe, accurate control of arm position.	X	X
2. Allow implementation as a robotic control system using traditional software and hardware configurations.	X	X
3. Contain tunable parameters to adjust the overall stiffness of the system, allowing adaptation to different tasks.	X	X
4. Operate about a set point and return to said set point after a perturbation.	X	X
5. Allow the addition of a bias torque to the output.	X	X
6. Be derived from and designed to simulate physiological characteristics.	X	
7. Be a commonly employed method of control.		X

Criterion 1, the stability of the control model, was of clear importance to this study. Safe interaction with a robot requires that the robot behave in a predictable, controllable fashion. Working or sharing an environment with unstable robots could prove hazardous for users.

As described by criterion 2, the model needed to allow implementation with standard hardware and software. This was to support the feasible implementation of the control models evaluated for this study in commercial applications without the need for custom hardware. Past studies have produced human-like robotic arms [Chou; 1994], but used purpose-built pneumatic actuators to achieve this performance. This approach is limited by the fact that the muscle properties are simulated by the mechanical properties of the actuator. This means that different muscles must be simulated with mechanically unique actuators to achieve the desired performance. By comparison, the same DC motor

controlled via software models can be easily reconfigured to simulate different muscles by changing model parameters in the software.

While the models used in this study only performed a single task, it is important that the models be tunable to adapt to different tasks as described in criterion 3. This feature is crucial if the models are to be used for a variety of tasks that could be encountered outside of this study. A robot supporting a load of several Newtons must have much stronger static stiffness than one supporting only a fraction of that load. Tunable parameters were also important in this study to produce steady-state and dynamic responses that, while influential on the performance of the subject, still required input from the subject to complete the task successfully. A model with high static and dynamic stiffness would reduce the relative contribution of the subject to a point where the subject becomes irrelevant. Conversely, the contribution of a too compliant system would become minimal with respect to the subject.

Criterion 4 dictated that the controller be able to operate about a set point and return to the set point after encountering a perturbation. This is an important characteristic in the context of this study as it has real-world implications. The exemplar team lift task requires that an object be lifted to a minimum height. If the object is perturbed, the team must return to the original set point before resuming the task. As such, it was necessary that the controller employed in this study be capable of returning to a set point after incurring a perturbation.

Adding bias torque to the models, as listed by criterion 5, was an important factor for this study to implement the virtual load described in section 4.1.

Finally, criteria 6 and 7 were specified to ensure that the biological model was representative of the physiological properties of muscle, and that the standard model was one that is commonly used as a control system.

4.2.3 PID Control Model:

The PID control scheme was chosen as the "standard" controller for this study because its simplicity of implementation and broad range of operating conditions [Guttirez; 2007]. Table 4.2 justifies the choice of this control model in the context of the criteria of table 4.1:

Table 4.2: PID model evaluation.

Criteria	PID Model
1. Remain stable after the onset of a perturbation to promote safe, accurate control of arm position.	When properly tuned, a PID algorithm is stable.
2. Allow implementation as a robotic control system using traditional software and hardware configurations.	PID control systems are commonly implemented in motor control systems.
3. Contain tunable parameters to adjust the overall stiffness of the system, allowing adaptation to different tasks.	Proportional, derivative, and integral gain can all be tuned to adjust stiffness and dynamic response of the system.
4. Operate about a set point and return to said set point after a perturbation.	The proportional and integral gains of the system can be set to ensure that the system will settle within the desired tolerance.
5. Allow the addition of a bias torque to the output.	A bias torque can be added at the output of a P or PD controller, but not PID.
6. Be derived from and designed to simulate physiological characteristics.	Not applicable.
7. Be a commonly employed method of control.	PID is the most common algorithm employed in automation [Guttirez, 2007].

In the context of this study, a tune-by-feel approach was not deemed appropriate, as the purpose of the standard control algorithm was to provide a reference against which to compare the human-like model. Common PID tuning schemes were examined to guide the tuning process for tuning of the PID algorithm (Table 4.3).

Table 4.3: PID tuning comparison chart.

Method	Advantages	Disadvantages
Tyreus-Luyben [Luyben; 1996]	Less aggressive, more robust tuning method than Ziegler-Nichols. Commonly used standardized tuning method.	Lower static stiffness than Ziegler-Nichols method, identification of parameters requires driving of system near instability.
Ziegler-Nichols [Ziegler et. al.; 1993]	Commonly used, proven method. Stiff position control.	Aggressive tuning means marginal stability in certain conditions. Setup requires the system to be driven to near instability by trial and error.
Cohen-Coon [Bequette; 2003]	Online method, no process upset necessary.	Only applicable to first-order processes, parameters not very robust
Software tools	Consistent, repeatable tuning.	Cost and training involved in implementation.
Tune by feel	No calculation required.	Results are subjective, could become unstable under some conditions.
Analytical design	Ensures stability, optimal control.	Requires thorough understanding of process models, no standardized method of parameter selection.

The Tyreus-Luyben and Ziegler-Nichols tuning methods share the advantage that the parameter selection is standardized, allowing for the repeatability of results in comparison to other tuning methods where parameter selection is decided by the designer. Both tuning methods are also widely used; a fact that realizes criterion 7 from the model selection list stating that a commonly employed method of control should be used.

The decision to use the Tyreus-Luyben method instead of the Ziegler-Nichols was based on the less aggressive nature of Tyreus-Luyben tuning. The relatively relaxed

tuning of the Tyreus-Luyben method reduces oscillatory behavior and increases

robustness over the Ziegler-Nichols method [Luyben; 1996]. The more robust

characteristics of the Tyreus-Luyben method are advantageous in unpredictable

situations, as simulated in this study, because the system can respond more predictably to

unforeseen disturbances.

Tuning via the Tyreus-Luyben method requires first driving the system to

oscillation. To do this, all PID gains are first set to zero. The proportional gain is then

increased in small steps and the system is subjected to an impulse. When the response of

the system becomes oscillatory, the value of the proportional gain is the critical gain, K_c.

The gains of the system are then defined as follows by the Tyreus-Luyben method

[Tyreus; 1996]:

$$K_P = \frac{K_c}{2.2}; \ \tau_I = 2.2 * P_V; \ \tau_D = \frac{P_V}{6.3} \qquad\qquad \text{Eq. 4.4}$$

where P_V is the period of oscillation of the system. The general control equation is then

given as a function of the error signal *e(s)* producing output torque *U(s)*:

$$U(s) = e(s)K_P\left(1 + \frac{1}{s\tau_I} + s\tau_D\right) \qquad\qquad \text{Eq. 4.5}$$

The critical gain and period of oscillation of the combined robot, board, and

passive human arm of one subject were found to be K_C=0.88 Nm/deg, and P_V=0.772 sec

respectively. These values were found experimentally through the standard method of

setting all gains to zero, then incrementally increasing the proportional gain and

subjecting the system to a step input until the system begins to oscillate. This yields

Tyreus-Luyben parameters of $K_P = 0.4$, $\tau_I = 1.698$ sec, and $\tau_D = 0.123$ sec.

Equivalently, the system can be represented by proportional, integral, and

derivative gains defined as:

$$K_P = \frac{K_c}{2.2}; \ K_I = \frac{K_P}{\tau_I} = \frac{K_P}{2.2 * P_V}; \ K_D = K_P \tau_D = \frac{K_P P_V}{6.3}$$

Eq. 4.6

For this system the PID gains were calculated to be $K_P = 0.4$ Nm/deg, $K_I = 0.236$

Nm/deg*s, and $K_D = 0.05$ Nm*s/deg. Because the encoder used in this study output a

digital signal (4096 lines per revolution), small steps in the encoder and error signal

produced noise in the derivative signal. A first-order low-pass filter with a 2 Hz corner

frequency was employed in the software to smooth the derivative of the error signal for

smoother, more stable control.

Furthermore, the actual implementation of the PID controller differed from the

theoretical description provided in the background discussion of PID controllers. The

application of a bias load required that the motor always produce a bias torque. The

integral control portion of the PID controller prevents the application of a bias torque at

the output because the torque from the integral portion of the controller will always

integrate to equal the opposite of the bias torque, resulting in zero net bias applied

through the motor. Therefore, the integral gain of the controller was set to zero,

effectively resulting in a PD controller. Limiting the PID controller to PD also makes the

controller similar to the human-like model as a PD algorithm is analogous to viscoelastic impedance, the same fundamental model used to describe the properties of muscle.
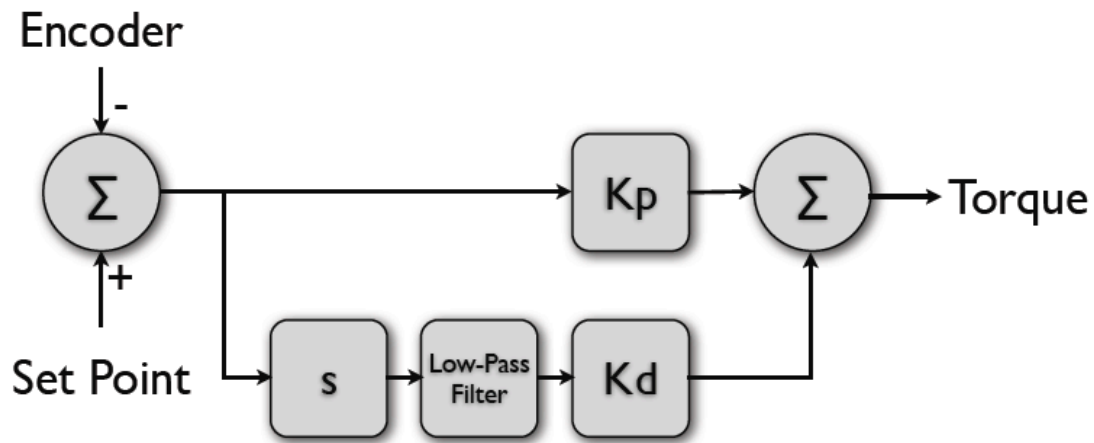
Figure 4.5: Actual PD implementation for the current study. Notably, a low-pass filter was added to the derivative loop for smoothing of the digital encoder feedback signal and the integral loop was removed to allow for the application of a bias torque.

4.2.4 Human-like model:

The human-like model used for this study combined a Hill-based muscle model, a reflex model, and a model of passive joint properties all acting in parallel. Simply using a muscle model would have resulted in a model that operates about a constant activation and would therefore only come to rest when the limits of the range of motion of the joint have been reached. This means criterion 4 of the performance requirements, stating the set point of the model can be set, would not be met. The addition of a reflex model ensures that the set point of the human-like model can be defined. Finally, a passive model simulated the non-linear elastic properties of the elbow joint. Passive damping properties were not included due to the arbitrarily small contribution to joint dynamics within the conditions of this study [Winters; 1985]. Table 4.4 lists how these models met the criteria set forth for the performance of the robotic control models.

31

Table 4.4: Neuromuscular model evaluation.

Criteria	Neuromuscular Model
1. Remain stable after the onset of a perturbation to promote safe, accurate control of arm position.	The neuromuscular model is inherently stable when parameter selection simulates a healthy neuromuscular system.
2. Allow implementation as a robotic control system using traditional software and hardware configurations.	This model has been successfully implemented in MATLAB/Simulink.
3. Contain tunable parameters to adjust the overall stiffness of the system, allowing adaptation to different tasks.	Modular design allows extensive flexibility in setting model parameters.
4. Operate about a set point and return to said set point after a perturbation. Model must be able to return within ±5° of the set point.	The set point for this model can be set through the reflex model.
5. Allow the addition of a bias torque to the output.	A bias torque can be added through the "descending command" block.
7. Be derived from and designed to simulate physiological characteristics.	Model based on extensive studies of the neuromuscular system.
8. Be a commonly employed method of control.	Not applicable.

4.2.4a Reflex Model:

Reflex model equations and parameters for this implementation were obtained from [Zhang, Rymer; 1997]. This model was particularly relevant to this study as the experimental protocol employed for model parameter identification closely resembled the goals of this study. Specifically, elbow flexion and extension reflexes were measured only under conditions without co-contraction as evidenced by EMG measurements [Zhang, Rymer; 1997]. Similarly in the current study, a bias torque is applied to eliminate co-contraction; therefore the operating conditions are very similar. This study also measured model parameters for varying background torques, making it possible to match reflex parameters to the background torque being produced by the robotic operator for a more accurate representation of reflex contributions.

The Zhang and Rymer study measured the contributions of limb viscosity (B), stiffness (K), and inertia (I) (Figure 4.6). The reflex response of the arm was modeled by the spindle properties as a feedback loop delayed by t_{d1} with proportional gain K_d and velocity gains r_p and r_n for lengthening and shortening respectively (lower loop of Figure 4.6). Finally, the contribution of the golgi tendon organ (GTO), a force-sensing element in series with the muscle, is modeled as a feed-forward loop delayed by t_{d2} and proportional to muscle torque. In the current study, only the spindle loop portion of the Zhang and Rymer model was used to predict the torque contribution of the reflex model. More detailed models were implemented for the passive and inertial properties as described in section 4.4.2b. The GTO contribution was not modeled as its contribution is relatively small over the small displacements encountered in this study [Chou, 1997].
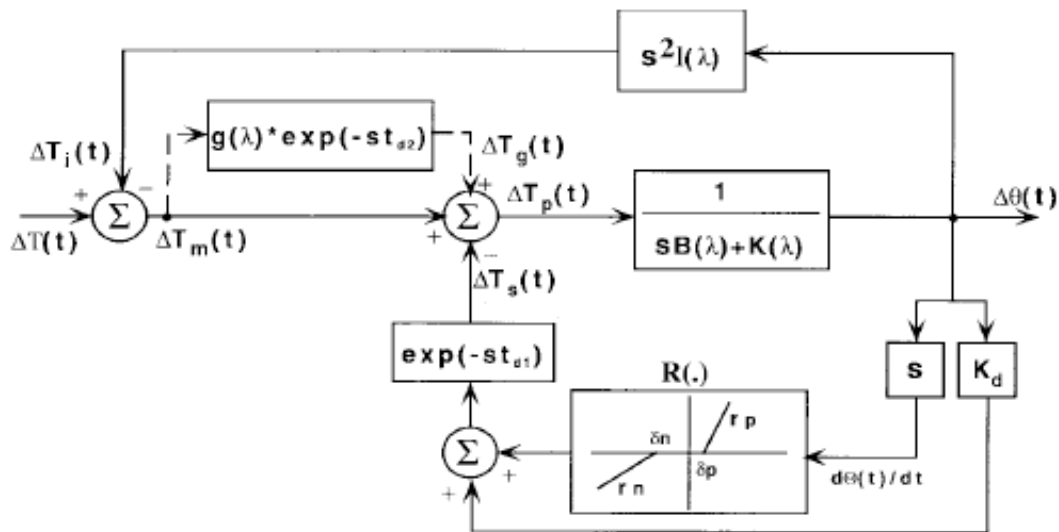
Figure 4.6: Joint model [Zhang, Rymer; 1997]. The stretch reflex is modeled by the lower proportional and derivative loops of the model.

33

It is important to note that while not explicitly modeled (figure 4.6), muscle contributions are included in the spindle reflex model. The high-level, lumped model (figure 4.6) can be separated into a more detailed model (figure 4.7), where *P* is the spindle contribution and *M* is the muscle contribution. In analyzing experimental data and defining their model, Zhang and Rymer note that the contributions of the spindle and muscle are not separated. Therefore the spindle loop shown in the high-level model (figure 4.6) is actually a lumped model of P and M from the more detailed model (figure 4.7). Similarly the descending command and GTO contributions are lumped with *M*, but are not used in the robotic controller for this study.
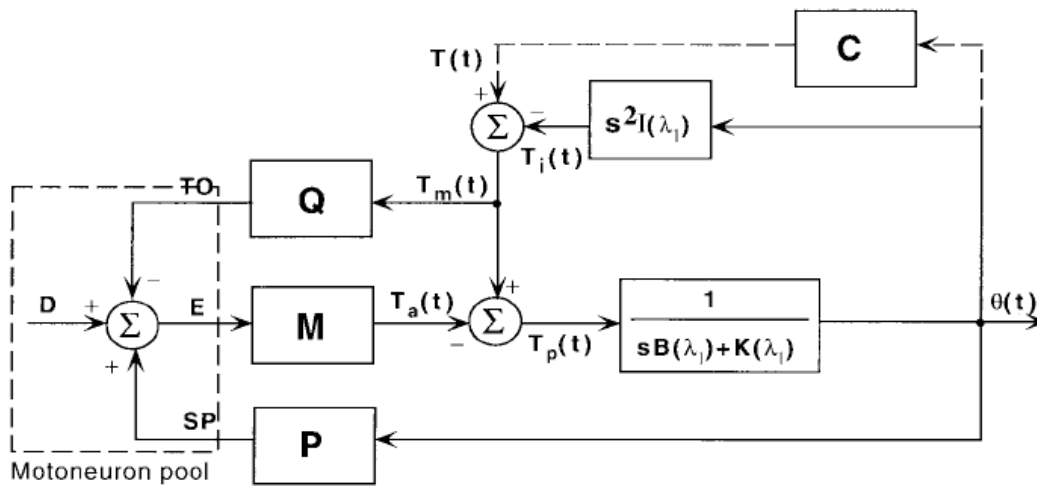
Figure 4.7: Expanded model. [Zhang Rymer 1997]

The parameters used to model the spindle contribution were t_{dl}, K_d, r_p, and r_n, all of which were estimated at 2.5 Nm of background torque. The values used were [Zhang and Rymer; 1997]:

t_{dl}=32 ms

K_d=0.07176 Nm/deg

r_p=0.00112 Nm*s/deg

r_n=0.0023 Nm*s/deg

4.2.4b Muscle Dynamics:

The muscle model and its parameters were obtained from [Winters; 1985] comprehensive joint models. The muscle models identified in this article are based on the Hill muscle model [Hill; 1938] and Wilkie's joint mechanical models [Wilkie; 1950]. The advantage of combining these two models is that parameters can be defined in terms of joint angles as opposed to muscle length in the Hill model. This is of interest in robotic implementation as feedback sensors report the joint angle and can therefore be sent directly to the model without requiring the additional calculation of muscle length from joint angle.

Another advantage of the parameters listed in the Winters study is that parameters are listed not only for individual muscles, but also as lumped parameters for a given joint along one degree of freedom (for example, the elbow has models for flexion and extension). This is ideal for implementation in robotic control as it allows the designer to scale the complexity of the model, if needed, according to available computational power by choosing to either model the individual muscles or defining models for the flexion and extension of a joint. For the current study in which the robotic operator is limited to elbow flexion, a single elbow flexion model was implemented instead of six separate models for the all the muscles crossing the elbow joint (long and short heads of the

Biceps, Brachialis, Pronator Teres, Brachioradialis, and Extensor Carpi Radialis [Gray; 1995]).

The behavior of the series elastic element is described as a non-linear spring [Winters; 1985]:

$$M(\theta) = (k_o * \theta_{se}) + \left[k_1 * (e^{k2*\theta_{se}} - 1) \right]; \quad \theta_{se} = \theta - \theta_{ce} \qquad \text{Eq. 4.7}$$

where M is the series-elastic torque, θ is the arm angle, θ_{ce} is the contractile element angle, θ_{se} is the series element angle, k_0=0.1 Nm/deg, and k_1 and k_2 are defined as:

$$k_1 = \frac{M_0}{e^{PE_{sh}}}; \quad k_2 = \frac{PE_{sh}}{PE_{xm}}; \qquad \text{Eq. 4.8}$$

where PE_{sh}=9 (unit-less) is the parallel shape parameter and PE_{xm}=90° is the displacement of the elbow joint at M_0, defining the range of motion.

Sensitivity analysis shows that the parallel viscoelastic element is most important outside of the "middle range" of joint angles and does not significantly contribute to stiffness in the normal operating range [Winters; 1985]. As such, the parallel element was not modeled in the robotic control system. Furthermore, over the relatively small operating range of less than ±10° in this study, the torque-angle property of the contractile element was found to vary by 0.2% at activation levels below 25% and was therefore considered to be a constant scaled by neural activation.

The torque-velocity property of the contractile element is comprised of two regions for lengthening and shortening conditions of the contractile element. The

equations for the torque-velocity relationship were adapted from [Winters; 1985] to take

torque as an input and output velocity. The modified equations for shortening and

lengthening are:

$$\textit{Shortening: } V_{ces} = \frac{B_h (T - M_0)}{C_h + T - M_0}$$

Eq. 4.9

$$B_h = MV_{sh} * (MV_{vm} - 0.5 * (1 - Nea)) * MX_{rat} = 6.91 \frac{rad}{\sec}$$

Eq. 4.10

$$C_h = Nea * M_{max} * (1 + MV_{sh}) = 15.84 Nm$$

Eq. 4.11

$$\textit{Lengthening: } V_{cel} = \frac{M_0 - T}{T - M_0 - MV_{shl}}$$

Eq. 4.12

where T is the overall torque produced by the muscle, M_0 is the isometric torque,

MV_{sh}=0.32 is a unit-less Hill shape parameter, MV_{vm}=22 rad/sec is the unloaded

maximum contractile velocity, Nea is the neural activation level (assumed to be 0.2 for

the purposes of this study), MX_{rat} is the length-tension property of the muscle (assumed to

be 1 for the small movements in this study), M_{max}=60 Nm is the maximum contractile

force of the muscle, and MV_{shl}=4.8 is the lengthening shape parameter [Winters; 1985].

The lengthening equation and shape parameter were modified from those published in

[Winters; 1985] as the published equations could not reproduce the published lengthening

curves. Equation 4.12 was based on the Winters lengthening equation, but modified to

replicate the published lengthening curves more accurately.

Because the muscle model is responsible for producing a bias torque as

implemented in this controller, the equations depicting muscle dynamics were solved for

a neural activation level of approximately 4.2%, corresponding to an isometric torque of 2.5 Nm.

4.2.4c Passive Plant Dynamics:

The series and contractile elements are placed in parallel with the passive joint properties to form a complete joint model. The passive plant dynamics were modeled similarly to the series-elastic element with the addition of a damping factor b_p:

$$M(\theta) = \left(k_p * \theta_{se}\right) + b_p * v + \left[k_1 * (e^{k2*\theta_{se}} - 1)\right]$$
Eq. 4.13

where k_p = 1.5 Nm/rad, b_p= 0.2 Nms/rad, and k_1 and k_2 are defined the same way they were in equation 4.8 with the same parameters [Winters, 1985].

4.3 Test Procedures

A total of 13 subjects, male (n=10) and female (n=3), were recruited to participate in the study as approved by the Washington State University Institutional Review Board. Subjects completed a total of 6 15-second static trials and 40 9-second dynamic trials. Subjects were instructed to hold the board in the neutral position, where their forearm was vertical, and maintain a constant activation level. During dynamic trials, subjects were given a "do not intervene" (DNI) instruction to prevent voluntary intervention after the onset of the perturbation and to simply maintain the same level of activation to return near the original operating point. The DNI instruction has been used extensively in reflex studies and has been shown to produce more consistent results by isolating the reflex response [Lewis et. al. 2006; Crago et. al. 1976].

4.3.1 Pre-trial preparation:

Prior to commencing the trials, dual-differential electromyography (EMG) electrodes connected to a desktop EMG system (Bagnoli 8 System; Delsys Inc.; Boston, MA) were placed on the short head of the biceps and lateral head of the triceps, and a reference electrode was placed on the ankle. The EMG data were low-pass filtered at 200 Hz using a first-order Chebyshev filter in post-processing. EMG was recorded as a means of verifying that co-contraction was not occurring during the trials.

The subject's wrist was splinted using an athletic wrist-guard to prevent any contribution from the wrist flexors or extensors. The upper arm was laid on a 30° wedge, at the base of which the elbow rested on a pad with a small ridge to prevent translation. Subjects were instructed to hold the board with their forearm in a vertical position, as verified by the investigator. The encoder for the robot was zeroed at that position to identify the set point about which the robot was to operate during the trials.

The subjects were allowed a series of practice trials to familiarize themselves with the forces to be expected during the trials. The investigator gave feedback if abnormalities appeared in the subject's EMG or movement patterns during this practice period.

4.3.2 Trial description:

The sequence of trials consisted of two static trials followed by twenty dynamic trials. Subjects were then allowed a short break of approximately 5 minutes to rest their

arms and then performed two static trials, twenty dynamic trials, and finally two more static trials. The robotic controller was chosen randomly before each trial and the subject was not informed of which controller was being used. Baseline EMG recordings were measured at the start and end of the testing sequence.

Static trials consisted of a 15-second period during which only the 2.5 Nm bias load was applied. Upon the verbal consent of the subject, the load was applied and the subject was given a 4-second period to return within $\pm 0.8°$ of the defined set point with the aid of visual feedback from an LED display. After the 4-second period, the visual feedback was turned off and the subject was instructed to hold a constant activation level to maintain position for the following 11 seconds.

Dynamic trials were 9 seconds long, starting with the same 4-second period to return to the set point after applying the bias load. After the 4-second return period a single 8 Nm, 35-millisecond perturbation occurred within a 4-second window after settling to the set point. The onset of the perturbation occurred randomly within the perturbation period to prevent the subject from anticipating the perturbation and habituating to the task over the course of the study. A 1-second buffer period was added to the end of the 4-second perturbation period to allow time to settle from perturbations that may have occurred late in the 4-second period.

<u>4.4 Performance Metrics</u>

To acquire an understanding of the quality of human-robot interaction in this study, performance measurements were chosen to reflect the static and dynamic properties of the human-robot team in a cooperative task. The static metrics were meant to describe how well the human-robot team was able to maintain a constant posture over a set time interval while the dynamic measurements described the ability of the human-robot team to respond to a perturbation.

The static measurements examined in this study quantified the drift of the human-robot team when subjected only to the virtual load; no perturbations were presented during static trials. The root-mean-square (RMS) and peak displacement static measurements were chosen due to their common application in postural evaluation studies [Zabjek et. al., 2005; Duval, 2006]. The mean operating point metric was chosen primarily to ensure that the human-robot team was operating within the same ranges for each controller. The static measurements (S1-S3) are described in table 4.5 and shown in figure 4.8.
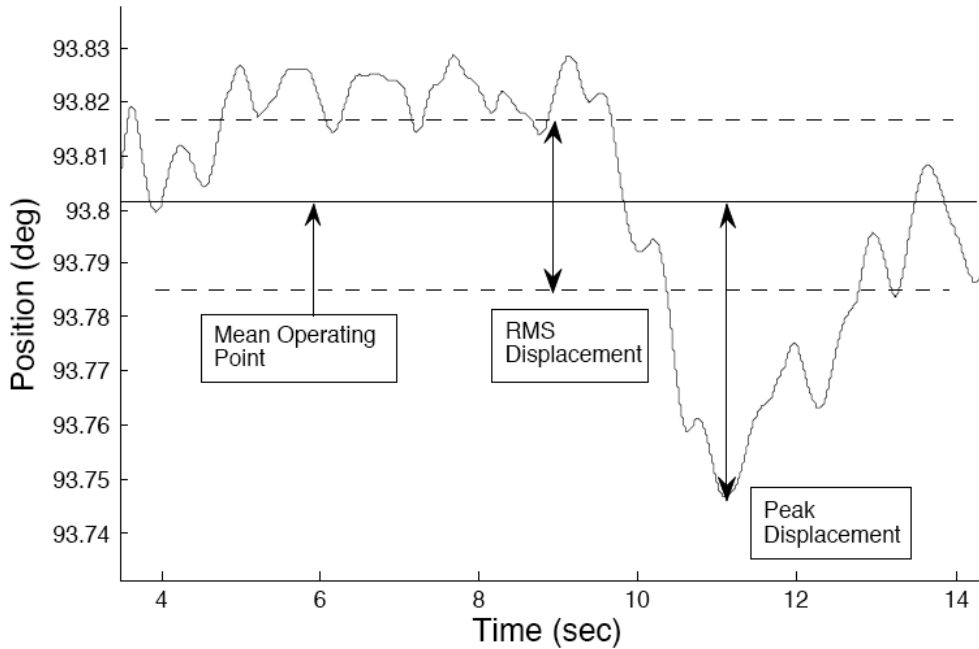
Figure 4.8: Static performance trial with metrics identified.

Table 4.5: Static performance metrics.

Metric	Description
S1. RMS Displacement	The root-mean-square displacement quantifies the amplitude of the drift experienced during the static trial, indicating the dispersion of the trajectory of the human-robot team during the postural task. The RMS displacement was measured after removing the mean from the data to indicate the spread of the drift.
S2. Peak Displacement	A measure of the maximum deviation from the set point during the postural task. Indicated the maximum boundaries within which the team operated. Peak displacement was measured as the distance from the mean of the data set.
S3. Mean Operating Point	Measurement of the mean operating point during the trial indicated how well the team could discern their position during the postural task.

The dynamic performance measurements quantified the behavior of the human-robot team when subjected to a perturbation. The measures examined the steady-state performance of the team during pre- and post-perturbation periods as well as the transient response immediately following the application of a perturbation. Peak displacement, settling time, and settling error are all common performance measurements used to evaluate control systems [Corriou; 2004] that were chosen for their relevance to the

42

performance of the postural task. The starting error metric was identified primarily to verify that trials for the two control models had comparable initial conditions.

Table 4.6 lists the measurements used to measure the dynamic response of the team (D1-D4). Figure 4.9 shows a visual description of the measurements on a typical trial position trace.
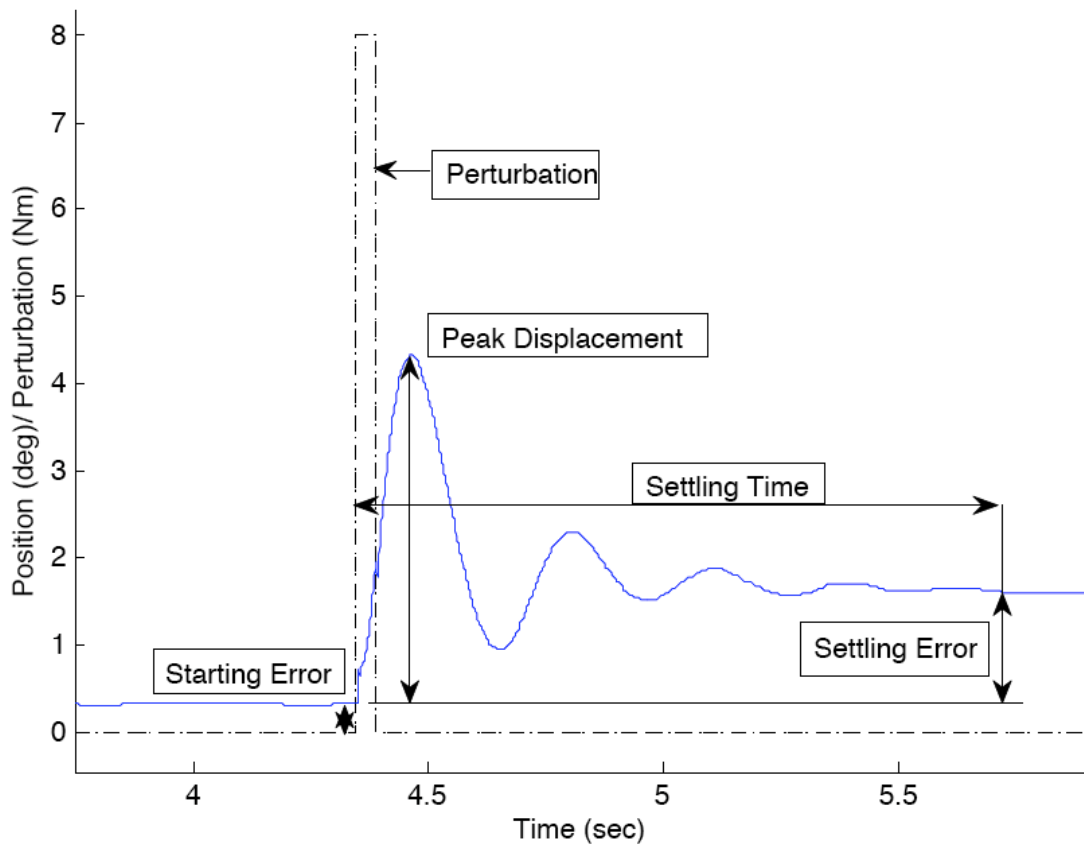
Figure 4.9: Typical dynamic trial with performance measurements identified.

Table 4.6: Dynamic performance metrics. D2-D3 were chosen for their popularity in evaluating control systems [Corriou, 2004] and their relevance to the postural task.

Metrics	Description
D1. Starting Error	A measurement of the position of the human-robot team immediately before the onset of the perturbation. Similar to the mean operating point measure for the static trials, but only evaluates position at one point in time.
D2. Peak Displacement	The maximum deflection caused by the perturbation. Displacement is measured as the distance between the peak displacement and the pre-perturbation position.
D3. Settling Time	Time required for the team to settle within 5% of peak velocity. This measure was chosen to be dependent on peak velocity instead of a constant value to compensate for the size of the displacement amplitude. Measured from the onset of the perturbation to the last time stamp exceeding 5% of peak velocity. Provides a measure of how quickly the team can recover from a perturbation.
D4. Settling Error	The difference between the settling position (measured at the same time stamp as the settling time) and the set point. Quantifies the ability of the human-robot team to return to the original operating point after being perturbed.

A set of variance metrics was also defined for the dynamic trials. This provided a measure of how consistent the performance of the human-robot team was over a series of trials. Consistency may be an important performance parameter in situations where predictability is of great importance. The variance measurements consist of measuring the coefficients of variation for each of the dynamic measurements (table 4.6) using equation 4.14.

$$c_v = \frac{\sigma}{\mu}$$ Eq. 4.14

where c_v is the coefficient of variation, σ is the standard deviation of the data from one control model for the subject, and μ is the mean of the data for that control model. The coefficient of variation provides a linear, normalized measure of the dispersion of the

data for each respective model [Krishnamurty et. al.; 1995], allowing for comparison between the dispersions of the two control models for consistency.

4.5 Detailed Hypotheses

As described in the experimental question chapter, the objective of this study was to compare the performance of the human-like controller to a standard control scheme, a PD controller. With the performance metrics identified, a more detailed list of hypotheses can be expressed for the static and dynamic performance of the human robot team (Table 4.7).

Table 4.7: Static performance hypotheses.

Metric	Null Hypothesis	Alternative Hypotheses
S1. RMS Displacement	H0: The mean RMS displacement of the human-like model is not significantly different from the mean RMS displacement of the PD controller	H1: The mean RMS displacement of the human-like model is significantly less than that of the PD controller.
		H2: The mean RMS displacement of the human-like model is significantly greater than that of the PD controller.
S2. Peak Displacement	H0: The mean peak displacement of the human-like model is not significantly different from the mean peak displacement of the PD controller	H1: The mean peak displacement of the human-like model is significantly less than that of the PD controller.
		H2: The mean peak displacement of the human-like model is significantly greater than that of the PD controller.
S3. Mean Operating Point	H0: The mean peak displacement of the human-like model is not significantly different from the mean RMS displacement of the PD controller	H1: The mean operating point of the human-like model is significantly less than that of the PD controller.
		H2: The mean operating point of the human-like model is significantly greater than that of the PD controller.

Two sets of dynamic measurement hypotheses were developed. One set (table 4.8) evaluated the measured performance of each model, while the second (table 4.9) compared the dispersion of the data for each model to evaluate consistency.

Table 4.8: Dynamic performance hypotheses.

Metric	Null Hypothesis	Alternative Hypotheses
D1. Pre-Perturbation Error	H0: The pre-perturbation error of the human-like model is not significantly different from that of the PD controller	H1: The pre-perturbation error of the human-like model is significantly less than that of the PD controller.
		H2: The pre-perturbation error of the human-like model is significantly greater than that of the PD controller.
D2. Peak Displacement	H0: The peak displacement of the human-like model is not significantly different from that of the PD controller	H1: The peak displacement of the human-like model is significantly less than that of the PD controller.
		H2: The peak displacement of the human-like model is significantly greater than that of the PD controller.
D3. Settling Time	H0: The settling time of the human-like model is not significantly different from that of the PD controller	H1: The settling time of the human-like model is significantly less than that of the PD controller.
		H2: The settling time of the human-like model is significantly greater than that of the PD controller.
D4. Settling Error	H0: The settling error of the human-like model is not significantly different from that of the PD controller	H1: The settling error of the human-like model is significantly less than that of the PD controller.
		H2: The settling error of the human-like model is significantly greater than that of the PD controller.

Table 4.9: Dynamic dispersion hypotheses.

Metric	Null Hypothesis	Alternative Hypotheses
D1. Pre-Perturbation Error (C.O.V.)	H0: The pre-perturbation error variance of the human-like model is not significantly different from that of the PD controller	H1: The pre-perturbation error variance of the human-like model is significantly less than that of the PD controller.
		H2: The pre-perturbation error variance of the human-like model is significantly greater than that of the PD controller.
D2. Peak Displacement (C.O.V.)	H0: The peak displacement variance of the human-like model is not significantly different from that of the PD controller	H1: The peak displacement variance of the human-like model is significantly less than that of the PD controller.
		H2: The peak displacement variance of the human-like model is significantly greater than that of the PD controller.
D3. Settling Time (C.O.V.)	H0: The settling time variance of the human-like model is not significantly different from that of the PD controller	H1: The settling time variance of the human-like model is significantly less than that of the PD controller.
		H2: The settling time variance of the human-like model is significantly greater than that of the PD controller.
D4. Settling Error (C.O.V.)	H0: The settling error variance of the human-like model is not significantly different from that of the PD controller	H1: The settling error variance of the human-like model is significantly less than that of the PD controller.
		H2: The settling error variance of the human-like model is significantly greater than that of the PD controller.

4.6 Analysis Methods

After completing their trials, all performance measurements described in section 4.2 were calculated. Before performing a statistical analysis on the results, each trial was compared against a series of rejection criteria to remove results from trials judged to have voluntary intervention for reasons described in chapter 2.

4.6.1 Rejection Criteria:

All data from a trial were disregarded if any of the rejection conditions were met. These rejection criteria include kinematic, EMG, and data distribution parameters to ensure that the subject followed instructions satisfactorily during that trial (figure 4.10).
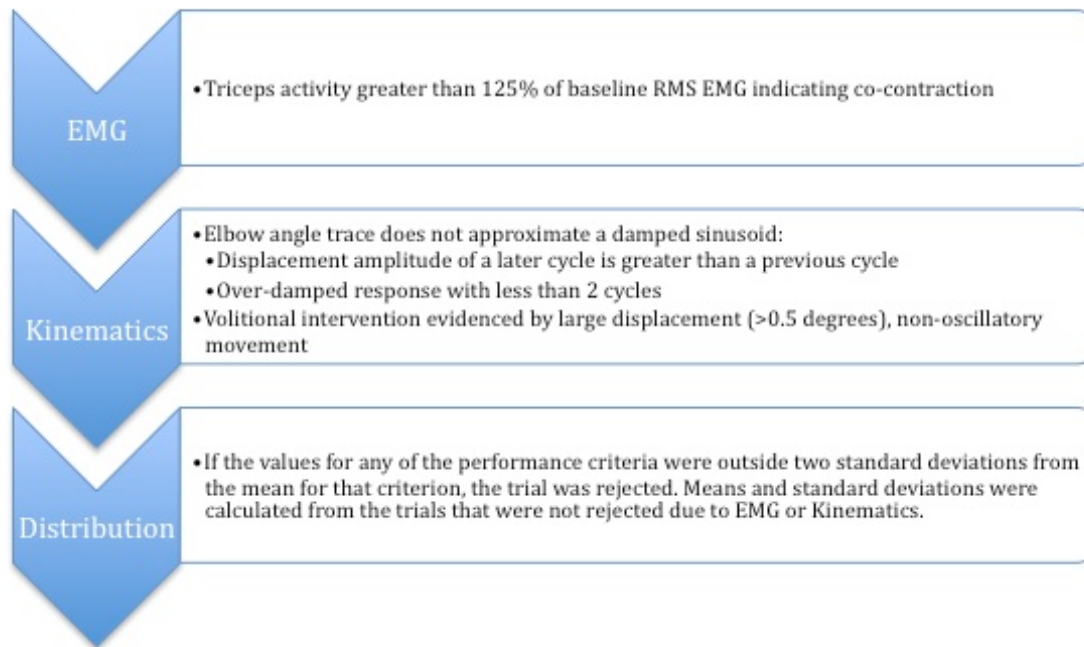
Figure 4.10: Rejection process and criteria.

The triceps EMG threshold level was chosen arbitrarily to detect co-contraction, but no trials outside of un-observed early practice trials showed any triceps EMG contribution, as expected from previous studies imposing a bias torque on limbs [Rymer & Zhang: 1997]. Criteria regarding voluntary intervention were obtained based on typical effects of voluntary intervention as identified in [Crago et. al.; 1976], specifically long time constant, large amplitude drift and heavy damping.

Each of the total six static trials, minus rejected trials, was considered as one data point for each of the performance metrics with the following information:

- RMS displacement (S1)

- Peak displacement (S2)

- Mean operating point (S3)

- Control scheme (Human-like or PD)

The forty dynamic trials, minus rejected trials, also each counted as a single data point for the performance metrics, producing up to forty data points per metric per subject. Each trial result included the following information:

- Pre-perturbation error (D1)

- Peak displacement (D2)

- Settling time (D3)

- Settling error (D4)

- Rectified settling error (calculated from D4)

- Control scheme

Because the direction (flexion or extension) of the settling error was not important in this study, the rectified settling error was used for analysis to prevent artificially small settling error means if a subject was equally distributed in both flexion and extension error between trials.

Finally, coefficients of variation were calculated for each of the performance metrics, providing one value per metric per subject.

4.6.2 Statistical Analysis:

4.6.2a Static trials

The results of the static trials for each subject were separated by control scheme, human-like and PD control, and averaged to provide one value per model per subject for each of the three static measurements. For each performance measurement, a paired t-test with an alpha of 0.05 was used to compare the means of each control model for each subject (n=11).

4.6.2b Dynamic Trials

The results of the dynamic trials were evaluated with a combination of parametric and non-parametric statistical tests due to inconsistencies in the variances measured. Variances for a given performance measure often differed between subjects as well as within subjects between control schemes. It was deemed insufficient to average the trials for each subject for comparison, as the potentially valuable variance information would be lost. To preserve the variance information a series of parametric tests identified whether a control scheme preference existed within a subject, then non-parametric tests evaluated the preferences of the subject population to determine whether a significant portion of the population shared the same preference.

First, an F-Test for variance (α=0.05) was performed to establish whether a significant difference existed in the variances of the two models for a given subject. The result of the F-test dictated the use of a t-test assuming either equal or unequal variances

(α=0.05). The outcome of the t-test provided a basis for categorizing the subject into one of four nominal categories for the given performance measure being analyzed (table 4.10).

Table 4.10: Preference categories.

Category	Definition
PD Preference	The mean performance of the PD model was significantly better than the human-like model.
BIO Preference	The mean performance of the human-like model was significantly better than the PD model.
PD No Preference	The mean performance of the PD model was better than the human-like model, but not statistically significant.
BIO No Preference	The mean performance of the human-like model was better than the PD model, but not statistically significant.

For all performance measurements, a smaller mean was considered better. Also, both no preference conditions are statistically equivalent, but were required for structuring the non-parametric analysis.

Preferences for the population were then tabulated for each performance metric and analyzed using Fisher's exact test (α=0.05). Because the sample population was less than 20 (n=13), Fisher's exact test was chosen over goodness-of-fit tests including χ^2 and the G-test that become inaccurate with small samples [Osborn, 2005]. Fisher's exact test was structured as shown in table 4.11:

Table 4.11: Fisher's exact test structure.

		Significant Preference		
		Yes	**No**	**Row Total**
Smaller Mean	**BIO**	a_{11}	a_{12}	$R_1=a_{11}+a_{12}$
	PD	a_{21}	a_{22}	$R_2=a_{21}+a_{22}$
	Column Total	$C_1=a_{11}+a_{21}$	$C_2=a_{12}+a_{22}$	$N=R_1+R_2=C_1+C_2$

Results from all 13 subjects were tabulated in the Fisher table and the critical p-value was calculated using equation 4.15.

$$p = \frac{(R_1!R_2!)(C_1!C_2!)}{N!(a_{11}!a_{12}!a_{21}!a_{22}!)}$$

Eq. 4.15

p-values for all possible combinations of $a_{i,j}$ achieving the same row and column totals were then calculated. The p-value for the Fisher test was then calculated by summing all p-values less than the critical p-value for the subject distribution. Possible outcomes for Fisher's exact test are listed in Figure 4.11.
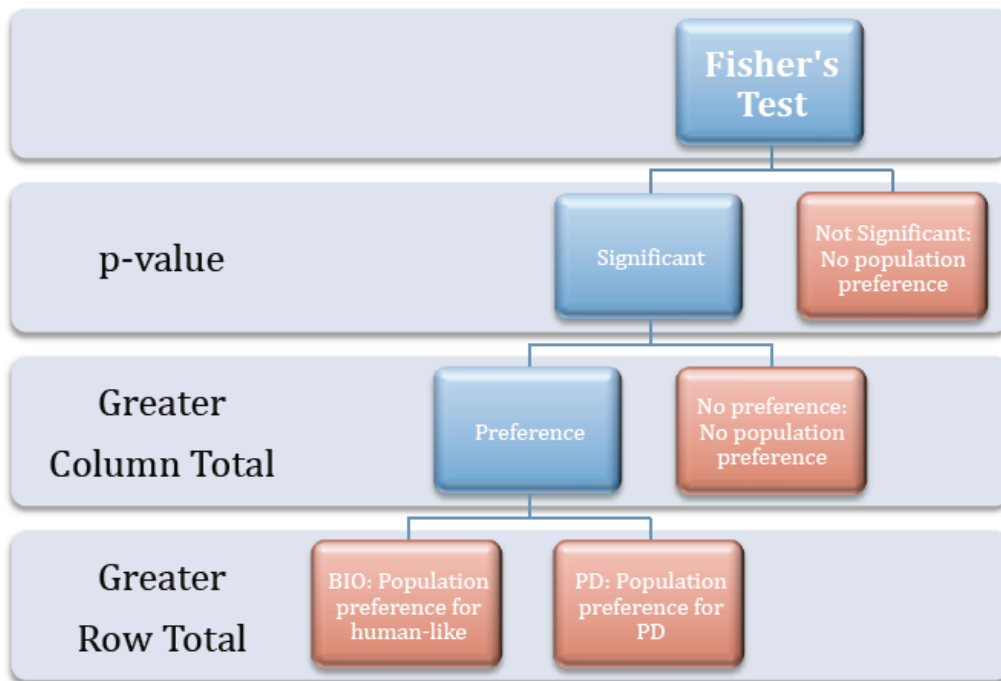
Figure 4.11: Fisher's exact test outcomes.

Consistency measurements were evaluated using the coefficients of variation calculated for each measure. C.O.V.s were calculated for each model for each subject and compiled into one data set in which each subject was one entry. The C.O.V.s for each model were then compared for the population using a paired t-test with α=0.05.

RESULTS

5.1 Static Trials

Data from 11 subjects were recorded for the static trials. Table A1-1 of Appendix 1 lists the average values of the three static performance measurements for each model of all 11 subjects. A typical static trial is plotted in figure 5.1 and population mean and standard deviation for each measurement are shown in figure 5.2. Of the total 66 static trials performed in this study, one was rejected due to apparent intervention.

For the static metrics, the RMS displacement measurement showed a significant difference (p=0.048) in the performances of the two models for the population, with the PD model resulting in smaller RMS displacement over the duration of the static trials (Figure 5.2). Results for the peak displacement test returned a p-value (p=0.079) near the significance threshold in favor of the PD model. The t-test performed on the mean operating point data indicated that there was no significant difference in the mean operating points of the two models. Detailed results of the paired t-tests are shown in table A1-2 of Appendix 1.
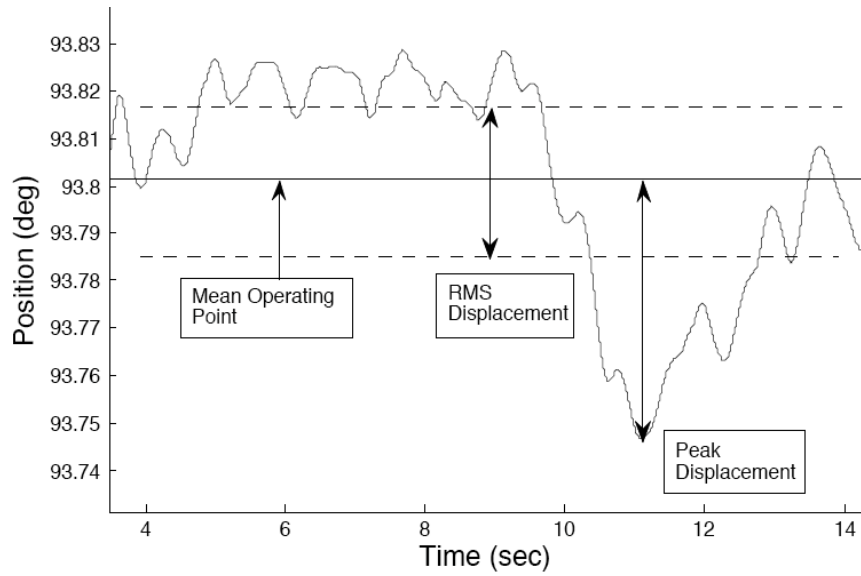
Figure 5.1: Typical static trial with performance metrics identified.
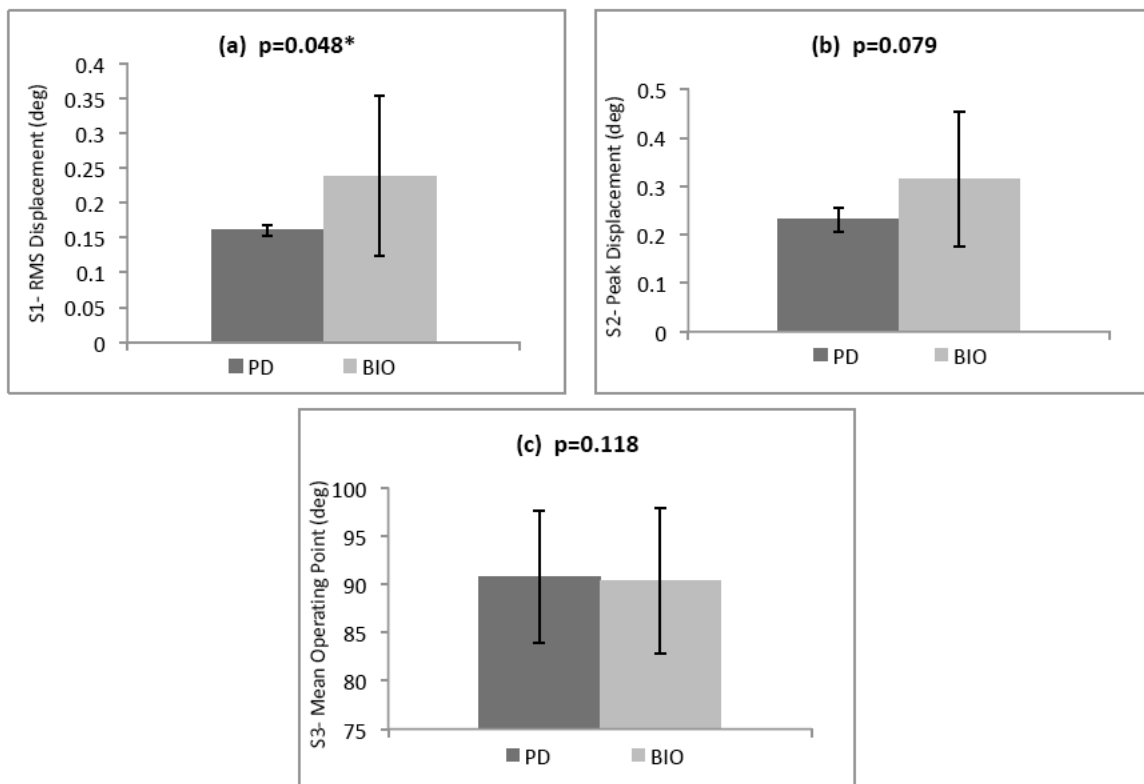
Figure 5.2: Population means for static measurements. Statistically significant results are identified with a star. (a): RMS displacement results. (b): Peak displacement results. (c): Mean operating point results.

5.2 Dynamic Trials

5.2.1 Performance Measurements Results:

Thirteen subjects performed a total of 40 dynamic trials, with 20 trials for each model. 10.9 of 40 trails (27%) were rejected per subject on average, with a range of 4 to 31 rejections (10%-78%), according to the rejection measurements. Figures 5.3 a-c show examples of trials rejected due to kinematic factors. Figure 5.3a displays a trial that was rejected due to volitional intervention, as evidenced by the slow return to position after settling from the perturbation between 4.6 and 7 seconds. Figure 5.3b shows an example of an over-damped trial, with all energy from the perturbation dissipated within the first cycle. Finally, figure 5.3c exemplifies a trial rejected when a later cycle exceeded the amplitude of a previous cycle. No trials were rejected due to improper EMG activation.

(a)
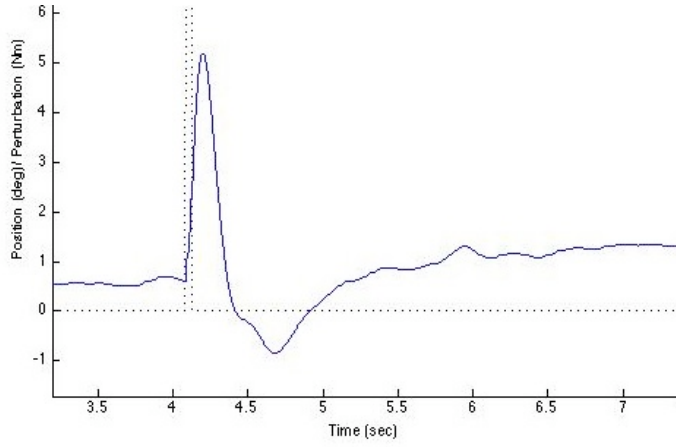
(b)
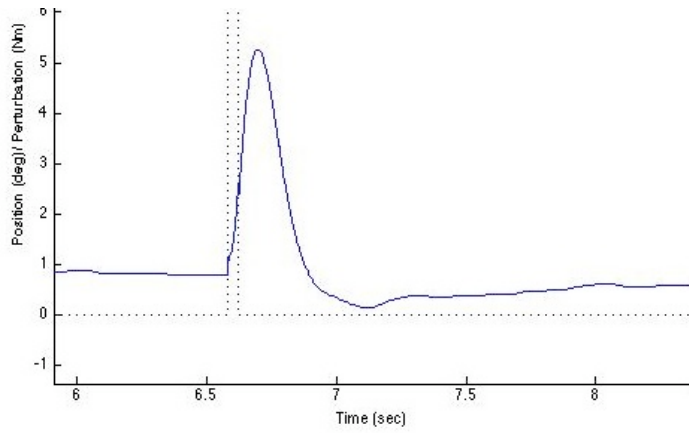
(c)
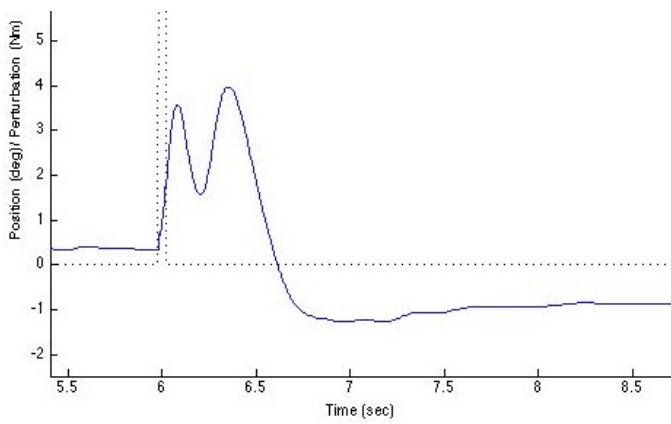
Figure 5.3 a-c: Exemplar rejected trials. (a): Volitional intervention. (b): Over-damped response. (c): Cycle amplitude exceeding previous cycles.

56

(a)
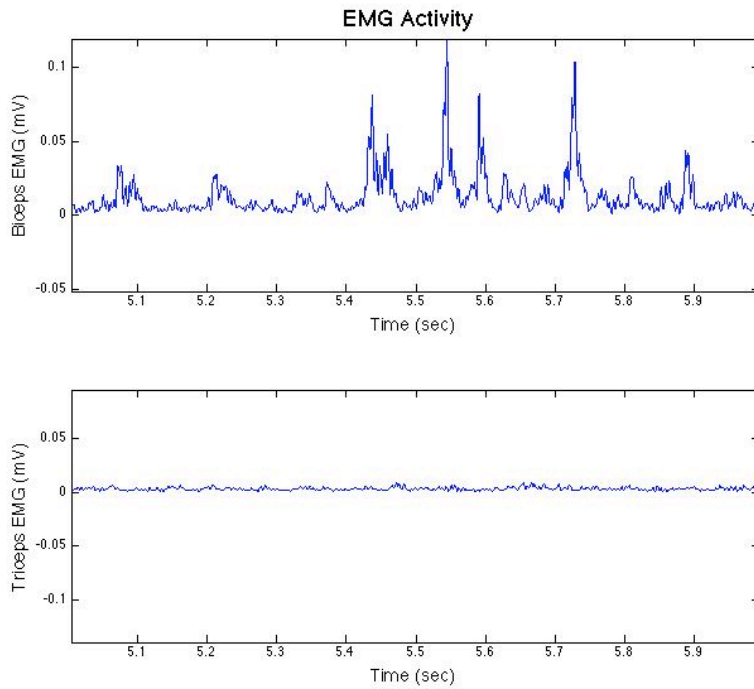
(b)
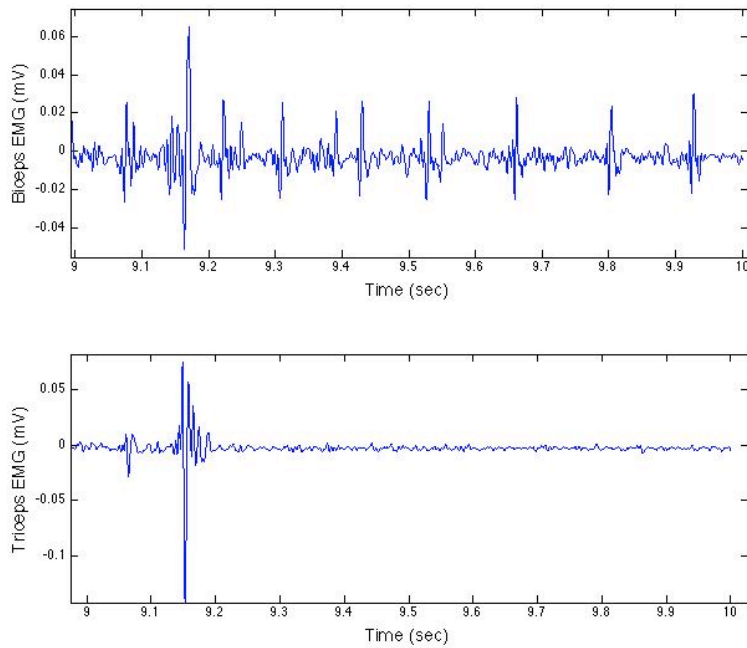
Figure 5.4 a,b: (a) EMG recordings of the bicep (top) and tricep (bottom) for a trial without co-contraction. Triceps co-contraction can be seen in (b) with a spike in EMG activity at approximately 9.15 seconds.

A typical perturbation trial is plotted in figure 5.5 to illustrate how measures were

obtained from a trial.
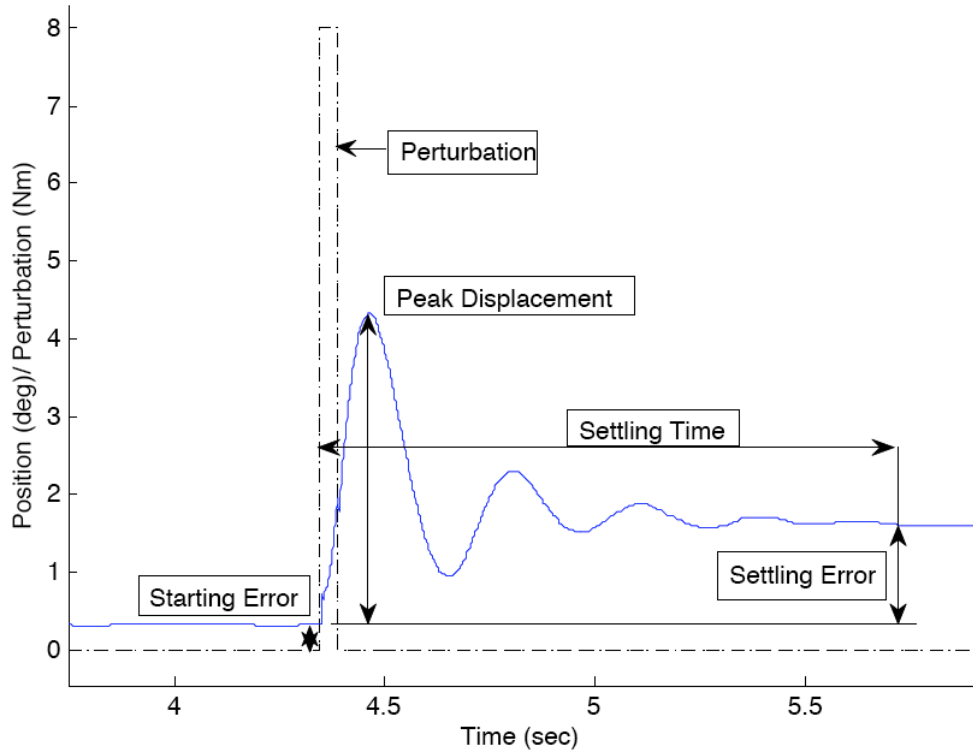
Figure 5.5: Typical acceptable perturbation trial with performance metrics identified.

The performances for each control algorithm were first compared using the F-test to establish whether the variances between the two algorithms were significantly different for each subject. Table A2-1 in Appendix 2 lists the F-test p-values for of the four performance measurements and table 5.1 summarizes the F-test results. The F-test results were used to individually define the assumptions of variance for each subject's t-test comparing the means of the two control algorithms. The p-values from the t-test indicated which model produced better performance; test results are listed in table A2-2 of Appendix 2 and summarized in table 5.2. Performance distributions are plotted in figure 5.6.

Table 5.1: F-Test results summary for dynamic trials listing significance of variances measured for each performance metric. Cells list the number of subjects falling in each of the three possible test outcomes (PD less variant, BIO less variant, or equal variance).

F-Test Result:	Performance Metric			
	Settling Time	Displacement Amplitude	Settling Error	Starting Error
PD < BIO ($p \leq 0.05$)	5	0	2	0
BIO < PD ($p \leq 0.05$)	2	1	0	0
BIO = PD ($p > 0.05$)	6	12	11	13

Table 5.2: T-Test results summary. Cells list the number of subjects in each of the three possible outcomes for each performance metric (PD mean significantly smaller, BIO mean significantly smaller, means not significantly different).

T-Test Result:	Performance Metric			
	Settling Time	Displacement Amplitude	Settling Error	Starting Error
PD < BIO ($p \leq 0.05$)	0	0	2	1
BIO < PD ($p \leq 0.05$)	2	13	1	0
BIO = PD ($p > 0.05$)	11	0	10	12
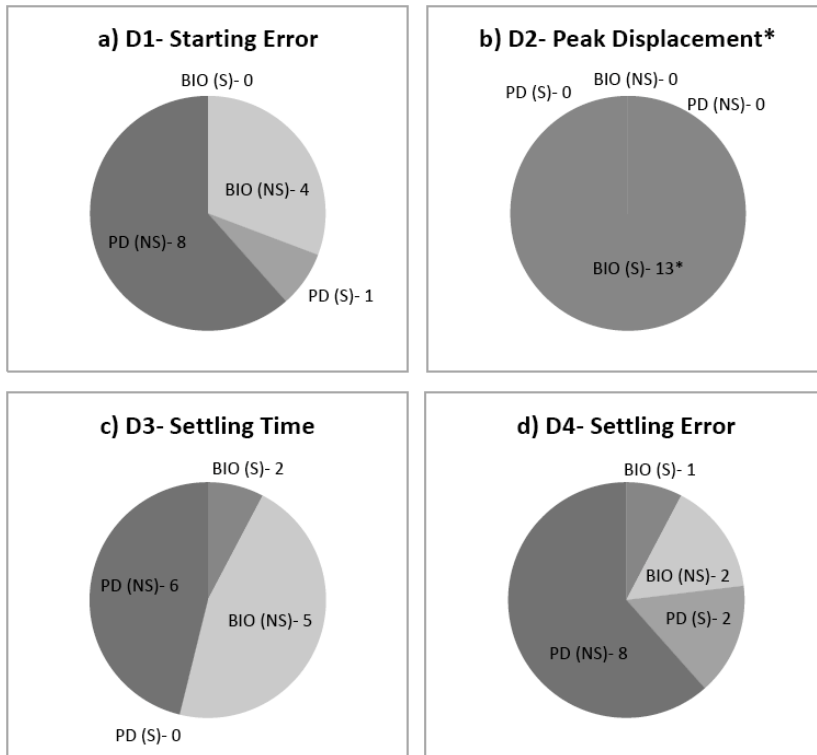
Figure 5.6 a-d: Population preference distributions. (S) categories identify the number of subjects that had a significantly smaller mean for that model, while (NS) categories contain the subjects that showed a smaller mean for the model, albeit not a significant difference between models. Distributions that showed a significant preference for one model across the population are identified with a star over the preferred category label.

59

The population preferences were then evaluated for significance using the non-parametric Fisher's exact test. The distribution tables, critical p-value, p-values for all alternative distributions, and resulting p-value are listed in table A2-3 of Appendix 2. Table 5.3 summarizes the results of Fisher's exact test. The distribution for the peak displacement measurement showed a significant preference for the human-like controller, while the other measurements showed no significant differences between controllers.

Table 5.3: Summary of Fisher's exact test p-values. Starred results are statistically significant.

	Starting Error	Peak Displacement	Settling Time	Settling Error
p-crit:	0.692	1.000	0.269	0.472
Test p-value:	0.308	0.000*	0.192	0.528

5.2.2 Consistency Evaluation:

The consistency of performance of each subject was measured for each control algorithm by comparing the coefficients of variation in each measurement for each controller. Table A2-4 in Appendix 2 lists the coefficients of variation calculated for each subject.

The coefficients of variation for each performance measurement were compared using a paired t-test. Figure 5.7 shows population mean and standard deviation for the four COV measurements. One test result, for settling time, showed a significantly smaller mean coefficient of variation for the PD model. All other measurements returned p-values that were not significant.
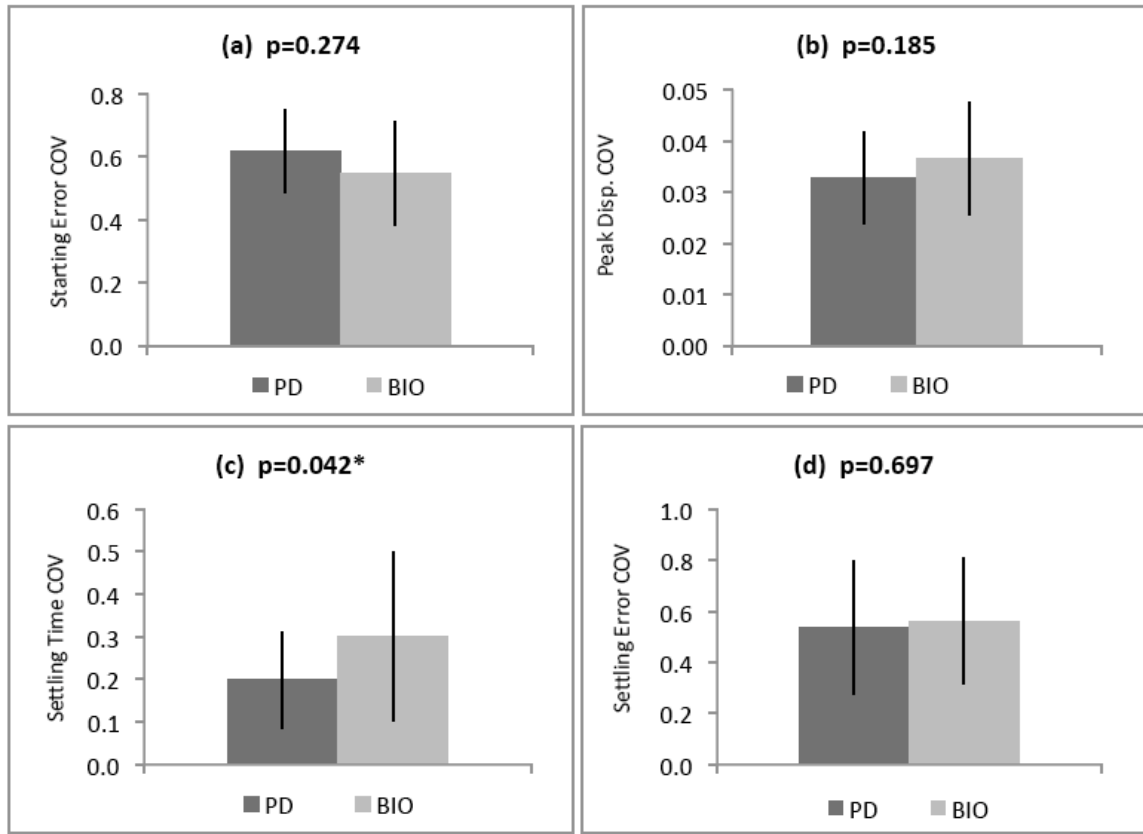
Figure 5.7: Mean and standard deviation of coefficient of variation results for dynamic measurements. Starred results are statistically significant.

DISCUSSION AND CONCLUSIONS

6.1 Control model performances

6.1.1 Static Trials

Performance measurement S3, mean operating point, served as a reference to ensure that the two control algorithms were operating about similar set points. The large p-value for the paired t-test on the mean operating point data confirms that the controller did not have a significant effect on the operating point. This is significant for two reasons; the computational models were both operating with similar mean inputs from the feedback sensors, and the human subjects were under the same operating conditions for both models. This ensured that the results measured arose from the mechanical impedances of the control algorithms and not from physically different operating conditions such as arms operating off-center with one model.

The two measurements with import in daily tasks were RMS and peak displacement, S1 and S2 respectively. While only the result from the RMS displacement test was significant (p=0.048), the result for the peak displacement was very close to the significance threshold (p=0.079). With less stringent confidence intervals of 90%, both results could have been significant. In both cases the PD algorithm showed smaller means, interpreted as better performance in the context of this study.

The results of the static tests have implications with respect to the performance of cooperative tasks. Postural tasks where steadiness is valued over movement speed or robustness could benefit from the reduced RMS excursion of approximately 30%. Both control models could be tuned to improve their static performance, the human-like model could make use of co-contracting reflex an muscle models, but stability is limited by delays in the reflex loop [Rymer, Hidler; 1999], while the PD algorithm could make use of more aggressive tuning like the Ziegler-Nichols method which utilizes higher stiffness parameters.

6.1.2 Dynamic Trials

As with the mean operating point metric for the static trials, the starting error metric verified that the dynamic trials for each model were comparable by ensuring the initial conditions were the same. Confirming equal initial conditions ensured that differences between models resulted from a difference in the cooperation of the human and robot, and not from the human operating along a different portion of the torque-angle curves. For example, if a model forced the starting position far from the neutral position, the static stiffness of the human operator would be smaller in a flexed or extended position than it would be in the neutral position [Winters; 1985]. Results for the starting error showed that all but one subject had statistically insignificant differences between the starting errors of the two models. As a population, the Fisher test showed that starting positions were equivalent for the two controllers.

The results for the peak displacement measurement overwhelmingly favored the human-like model with all 13 subjects showing a significant preference for the human-like model. The result of the Fisher test supported that, as a population, the human-like model outperformed the PD algorithm. The other two metrics, settling time and settling error, showed no significant differences as a population with most subjects showing no preference for one model. Notably, the settling time distribution skewed slightly towards the human-like model with two subjects preferring human-like versus zero for PD, but the result was not statistically significant.

The non-linear properties of the anthropomorphic model were therefore able to reduce peak displacement significantly without affecting settling time. In a linear PD controller, increasing derivative gain to reduce peak displacement necessitates a trade-off for longer settling times in response to an impulse [Robinett et. al.; 2001]. The damping properties of muscle are such that damping will increase in response to increasingly large perturbations, reducing the displacement amplitude. This allows for more aggressive dissipation of large perturbations where dissipation is more critical while leaving smaller displacements relatively lightly damped where a persistence of small oscillations is physiologically acceptable [Lin, Rymer; 2001]. This characteristic can also explain the small, but statistically significant ($p=0.042$), advantage in settling time consistency measured with the PD model since the damping factor was consistent across all trials.

6.2 Study Design Considerations

It is important to note that the integral control was removed from the PD algorithm. The integral control is responsible for reducing steady-state error in automation systems, and would have reduced the steady-state error in the dynamic trials and RMS displacement for static trials, but affected dynamic performance negatively with increased oscillatory behavior and overshoot. The exclusion of integral control was necessary to ensure that the two control schemes were comparable in this study, but the implications of integral control should be considered depending on the task being performed. In many daily tasks, integral control achieving zero steady-state error is unnecessary, and potentially harmful in that obstructions are not differentiated from error caused by process parameters such as gravity or friction [Mason, 1982; Drake, 1977; Whitney, 1982]. As such, the integral loop could increase force until saturation or damage occurs to the environment or robot.

The biologically inspired model implementation combined a variety of models for the muscle, reflex, and passive joint properties. The Winters models for muscle and joint properties [Winters; 1985] were ideal for implementation in this robotic operator as they provided models adapted from the classical Hill muscle model with specific parameters for the relevant joints. Some simplifications were necessary, however, to implement the model in this control system. Small angle approximations were made in some of the muscle model equations described in chapter 4 as a direct implementation of the described equations resulted in mathematical errors, such as division by zero, during the simulation. Unlike human muscle, the muscle model incorporated in the robotic

controller acted about a constant activation level with force modulation coming from a reflex model in parallel with the muscle instead of the reflex modulating the activation of the muscle. This configuration was necessary because of the increments of the digital signal were amplified by the derivative portion of the reflex model and created instabilities in the muscle model. This design was considered justifiable in this situation because of the small displacements encountered during perturbation trials, but the non-linearities in the biological models mean that parallel muscle and reflex models would show less fidelity towards human neuromuscular systems in applications seeing larger displacements [Strogatz; 2000].

6.3 Implications

The results have shown that subjects interacting with the PD controller had an advantage in static metrics while the anthropomorphic controller provided benefits in dynamic performance. In the context of this study, a smaller mean was considered advantageous for all performance metrics, as the goal for the human-robot team was to hold a load in a constant position. This instruction places value on smaller displacements from, and shorter return times to the operating point. When designing a robot for human cooperation, consideration must be given to the performance criteria and how the results measured in this study apply to the scope of the tasks. It is important to establish which criteria are relevant and whether the smaller means that were advantageous in the current task are beneficial or detrimental for the new instruction.

Traditional automation practice places high importance on stiffness, critical damping, and reducing steady-state error [Liptak; 2003]. In contrast to this, the human neuromuscular system behaves as a compliant, viscoelastic impedance with varying stiffness and damping properties depending on the task and goals [Crago et. al.; 1976]. The results of this study have shown that for a cooperative postural task, the human-like controller behaved in a more compliant, stable manner than the PD controller, while the PD controller allowed precise steady-state performance and improved consistency.

6.4 Potential Mechanisms

In evaluating the quality of HRI in this study, one possible outcome was that an anthropomorphic controller would shift the operational state of the human subject, as defined by the amplitude and frequency dependent stiffness of the intrinsic and reflex properties of muscle [Brown, 1982; Joyce, 1974], to a more or less optimal state than the traditional controller. In this study, the differences between controllers, while statistically significant for some metrics, were too subtle to effect a change in the operation of the human subject. For example, the frequency content of kinematic data from the static trials was comparable (figures 6.1 and 6.2), implying that the controller did not affect the operating point frequency of the system significantly.
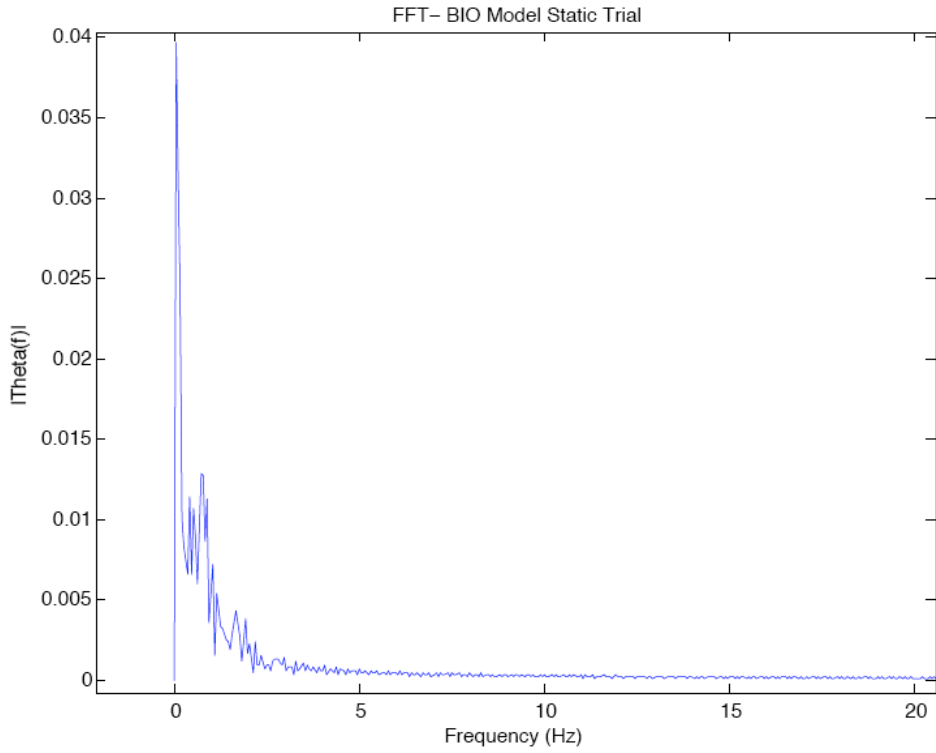
Figure 6.1: Frequency distribution of a typical static trial with the anthropomorphic controller.
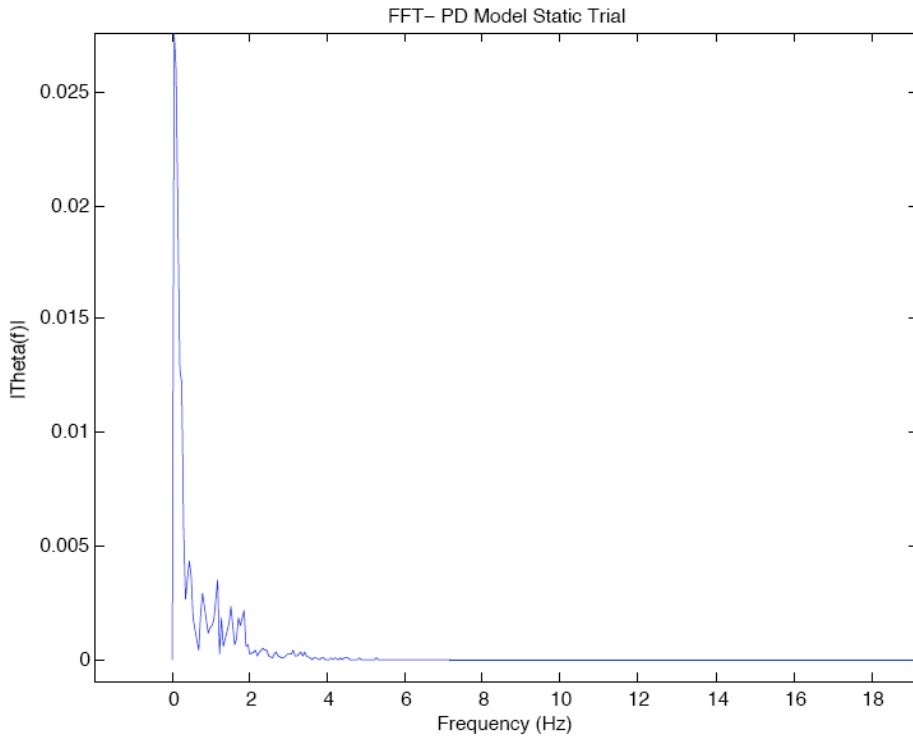
Figure 6.2: Frequency distribution of a typical static trial with the PD controller.

68

A PD controller with a stiffer proportional component, for example one determined by the Ziegler-Nichols method, may have yielded a significantly increased frequency of motion and thus affected the frequency-dependent properties of the stretch reflex by reducing the viscosity of the human impedance [Joyce; 1974]. Amplitude differences between controllers were significantly different for static trials where the PD controller showed smaller amplitudes, and for dynamic trials where the anthropomorphic model exhibited smaller peak displacements. While significant, these results were once again too subtle to elicit a change in the operational state of the human, the differences were only one-quarter of one degree for amplitude in dynamic trials and eight-hundredths of one degree for RMS displacement in static trials.

As previously discussed in section 2.2, this study provided two complementary pathways for the robotic controller to affect the outcomes of the trials; through its own independent performance characteristics, and by causing a shift in the operational state of the human subject. Due to the minimal differences in the frequency and amplitude parameters, it is not possible to justify stating that the human subjects were affected during the course of the trials. Therefore, the significance of the results are likely controller dependent and not the result of synergy between the human and robot, the PD controller is a slightly stiffer controller allowing less excursion during steady-state trials, while the anthropomorphic controller has nonlinear properties that can reject disturbances more effectively.

6.5 Roadmap for Physical HRI Studies

Two experimental design decisions of this study suggest direction for future research in the study of physical HRI, controller tuning and task type. The task and controllers chosen for this study were selected to gain insight into the fundamental intrinsic and reflexive characteristics of interaction. To examine these properties, a linear PD controller was selected with properties similar to those of biological models and a task was chosen that involved no voluntary contributions from the human subject.

The selection of the PD controller tuned with Tyreus-Luyben parameters was based on the robust design of the tuning scheme making it a likely candidate for implementation in robots performing daily tasks. This meant a relatively compliant tuning scheme with properties that, while linear, were similar to the biological model under the small displacements and velocities encountered in this study. While this made for a comparison of like controllers, it also resulted in small changes in the kinematics of the trials, therefore having little effect on the human subjects. Future research into the physical aspects of HRI should consider more aggressive tuning schemes, such as the Ziegler-Nichols method, during a similar postural task to determine whether a dramatically different linear controller would modify the response from the human subject.

The postural task in this study was designed specifically to prevent voluntary intervention. The lack of voluntary intervention allowed for the clear observation of intrinsic and reflexive components without the variability of voluntary modulation. While

an understanding of the intrinsic and reflexive properties of interaction provides a necessary foundation for future study of cooperation, voluntary interaction between humans and robots have previously shown the greatest potential for differentiation between anthropomorphic and standard robotic design schemes [Breazeal; 2003]. Volitional adaptation to the novel impedance characteristics of a PID controller could show significant differences from anthropomorphic control models that emulate impedances that the subject is familiar with from peer to peer interaction.

BIBLIOGRAPHY

Adams, Julie A. "Critical Considerations for Human-Robot Interface Development."
    AAAI Fall Symposium: Human Robot Interaction Technical Report.
    Massachusetts, North Falmouth. 15 Nov. 2002.

Bequette, B. W. Process Control : Modeling, Design and Simulation. Upper Saddle
    River: Prentice Hall PTR, 2003.

Boyd, Robert. Solving the Puzzle of Human Cooperation. Diss. University of California
    Los Angeles, 2000. Los Angeles, CA: UCLA, 2000.

Breazeal, Cynthia, Andrew Brooks, and Et. Al. "Humanoid Robots as Cooperative
    Partners for People." 13 Dec. 2003. 21 Aug. 2007
    <http://www.ee.pdx.edu/~mperkows/class_robotics/febr26-
    2004/humanoids/robot-partner-breazeal-etal-ijhr04.pdf>.

Bronzino, Joseph D. Biomedical Engineering Fundamentals. New York: C R C P LLC,
    2006. 8:13-8:15.

Brown, T. H., P. H. Rack, and H. F. Ross. "Forces Generated at the Thumb
    Interphalangeal Joint During Imposed Sinusoidal Movements." Journal of
    Physiology 332 (1982): 69-85.

Bruce, Allison. "The Role of Expressiveness and Attention in Human-Robot Interaction."
    IEEE, IEEE International Conference on Robotics & Automation, May 2002,
    Washington, DC. Robotics & Automation 2002. Vol. 4. IEEE, 2002. 4138-142.

Chiari, Lorenzo, and Et. Al. "An Improved Technique for the Extraction of Stochastic
    Parameters from Stabilograms." Gait and Posture 12 (2000): 225-34.

Chou, Ching-Ping, and Blake Hannaford. "Study of human forearm posture maintenance
    with a physiologically based robotic arm and spinal level neural controller."
    Biological Cybernetics 76 (1997): 285-98.

Clauser, Charles E. Weight, Volume, and Center of Mass of Segments of the Human
    Body. United States. Air Force. Systems Command. OH: Wright Patterson
    A.F.B., 1969.

Close, R. I. "Dynamic Properties of Mammalian Skeletal Muscles." Physiol. Rev. 52
    (1972): 129-97.

Collins, J. J., and C. J. De Luca. "The Effects of Visual Input on Open-Loop and Closed-
    Loop Postural Control Mechanisms." Experimental Brain Research 103 (1995):
    151-63.

Corriou, Jean-Pierre. <u>Process Control</u>. New York: Springer, 2004. 130.

Crago, P. E., J. C. Houk, and Z. Hasan. "Regulatory actions of human stretch reflex." <u>Journal of Neurophysiology</u> 39 (1976): 925-35.

Crandall, Jacob, and Et. Al. "Validating Human-Robot Interaction Schemes in Multi-tasking Environments." <u>IEEE Transactions on Systems, Man, and Cybernetics-Part A</u> 35 (2005): 438-49.

Drake, S. H. <u>Using Compliance in Lieu of Sensory Feedback for Automatic Assembly</u>. Diss. Massachusetts Institute of Technology, 1977. Cambridge, MA: Dept. Mechanical Engineering, 1977.

Duval, Christian, and Loretta Norton. "Tremor in Patients with Migraine." <u>Headache: The Journal of Head and Face Pain</u> 46 (2006): 1005-010.

Eaton, Robert C., ed. <u>Neural Mechanisms of Startle Behavior</u>. New York: Basic Books, 1984. 287-88.

Feng, C. J., and A. F. Mak. "Neuromuscular model for the stretch reflex in passive movement of spastic elbow joint." Engineering in Medicine and Biology Society, Proceedings of the 20th Annual International Conference, Oct. 1998, Washington, DC. <u>IEEE Engineering in Medicine and Biology Society</u>. Vol. 5. IEEE. 2317-320.

Ganong, William F. <u>Review of Medical Physiology</u>. New York: Appleton & Lange, 2003.

Gates, William. "A Robot in Every Home." <u>Scientific American</u> 1 Dec. 2006: 1-5.

Gray, Henry. <u>Gray's Anatomy : The Classic Collector's Edition</u>. New York: Gramercy Books, 2001.

Guttirez, Javier. "Proportional-Integral-Derivative Explained." <u>Industrial Control</u>. 13 Apr. 2007. Techonline. 28 Oct. 2008 <http://www.industrialcontroldesignline.com/howto/199000752>.

Hidler, J. M., and W. Z. Rymer. "A simulation study of reflex instability in spasticity: origins of clonus." <u>IEEE Transactions on Rehabilitation Engineering</u> 7 (1999): 327-40.

Hill, A. V. "The Heat of Shortening and the Dynamic Constants of Muscle." The Royal Society, Series B, Biological Sciences, Oct. 1938. <u>Proceedings of the Royal Society of London.</u> London: The Royal Society, 1938. 136-95.

Hogan, Neville, and Ferdinando Mussa-Ivaldi. "Integrable Solutions of Kinematic Redundancy via Impedance Control." <u>International Journal of Robotics Research</u> 10 (1991): 481-91.

Joyce, G. C., M. H. Rack, and H. F. Ross. "The Forces Generated at the Human Elbow Joint in Response to Imposed Sinusoidal Movements of the Forearm." <u>Journal of Physiology</u> 240 (1974): 351-74.

Kearney, R. E., R. B. Stein, and L. Parameswaran. "Identification of intrinsic and reflex contributions to human ankle stiffness dynamics." <u>IEEE Transactions on Biomedical Engineering</u> 44 (1997): 493-504.

Klute, Glenn, Joseph Czerniecki, and Blake Hannaford. "Artificial Muscles: Actuators for Biorobotic Systems." <u>International Journal of Robotics Research</u> 21 (2002): 295-309.

Krischnamurty, Goteti B., David Ostroff, and Patricia Kasovia-Schmitt. <u>Statistics : An Interactive Text for the Health and Life Sciences</u>. New York: Jones & Bartlett, Incorporated, 1995.

Lan, Ning. "A Biomechanical Model of Arm Postural Control By Functional Electrical Stimulation." IEEE, Engineering in Medicine and Biology Society Annual Conference, Sept. 1995. <u>Eng. in Med. and Biol. Soc.</u> Vol. 2. IEEE, 1995. 1151-152.

Laumond, Jean-Paul. <u>Robot Motion Planning and Control; Compliant Motion</u>. Ed. M. T. Hammond. New York: Springer, 1982. 305-22.

Lewis, G. N., C. D. MacKinnon, and E. J. Perreault. "The effect of task instruction on the excitability of spinal and supraspinal reflex pathways projecting to the biceps muscle." <u>Experimental Brain Research</u> 174 (2006): 413-25.

Lin, David, and William Rymer. "Damping Actions of the Neuromuscular System with Inertial Loads: Human Flexor Pollicis Longus Muscle." <u>Journal of Neurophysiology</u> 85 (2001): 1059-066.

Liptak, Bela G., ed. <u>Instrument Engineers' Handbook</u>. New York: CRC P, 2003. 108-13.

Luyben, W. L. "Tuning proportional-integral-derivative controllers for integrator/deadtime processes." <u>Industrial & Engineering Chemistry Research</u> 35 (1996): 3480-483.

Minato, Takashi. <u>Development of an Android Robot for Studying Human-Robot Interaction</u>. Diss. Osaka University, 2004. Osaka, Japan.

Mussa-Ivaldi, Ferdinando, Neville Hogan, and E. Bizzi. <u>Journal of Neuroscience</u> 5 (1985): 2732-743.

Norman, Donald A. <u>The Design of Everyday Things</u>. New York: MIT P, 1998.

O'Dwyer, Aidan. <u>Handbook of PI and PID Controller Tuning Rules</u>. New York: Imperial College P, 2003. 6-9.

Ouyang, P. R., W. J. Zhang, and F. X. Wu. "Nonlinear PD Control for Trajectory Tracking with Consideration of the Design for Control Methodology." IEEE, International Conference on Robotics & Automation, May 2002, Washington, DC. <u>Robotics & Automation 2002</u>. Vol. 4. IEEE. 4126-131.

Perreault, E. J., P. E. Crago, and R. F. Kirsch. "Estimation of intrinsic and reflex contributions to muscle dynamics: a modeling study." <u>IEEE Transactions on Biomedical Engineering</u> 47 (2000): 1413-421.

Reed, Kyle, Michael Peshkin, Edward Colgate, and James Patton. IEEE, IEEE International Conference on Robotics and Automation, Apr. 2004, New Orleans, LA. <u>IEEE Xplore</u>. 26 Apr. 2004. IEEE. 9 Sept. 2008 <http://ieeexplore.ieee.org/xpl/freeabs_all.jsp?arnumber=1307410>.

Reeves, Byron, and Clifford Nass. <u>The Media Equation</u>. 1st ed. Vol. 1. Stanford, CA: CSLI Publications, 1996.

Robinett, Rush D., Clark Dohrmann, and G. R. Eisler. <u>Flexible Robot Dynamics and Controls</u>. New York: Springer, 2001. 235.

Sidner, Candace, and Et. Al. "Where to Look: A Study of Human-Robot Engagement." Association for Computing Machinery, International Conference on Intelligent User Interfaces, 2004, Funchal, Portugal. <u>Proceedings of the 9th Conference on Intelligent User Interfaces</u>. Vol. 9. New York, NY: ACM, 2004. 78-84.

Strogatz, Steven H. <u>Nonlinear Dynamics and Chaos : With Applications to Physics, Biology, Chemistry, and Engineering</u>. New York: Perseus Books Group, 2000. 150.

Su, Chun-Yi, Subhash Rakheja, and Enrong Wang, eds. <u>Advances in Dynamics, Instrumentation and Control : Proceedings of the 2004 International Conference (CDIC '04) Nanjing, China 18 - 20 August 2004</u>. Boston: World Scientific Company, Incorporated, 2004. 103-06.

Trafton, Gregory J., and Et. Al. "Enabling Effective Human-Robot Interaction Using Perspective-Taking in Robots." <u>IEEE Transactions on Systems, Man, and Cybernetics- Part A</u> 35 (2005): 460-70.

Tyreus, B. D., and M. L. Luyben. "Analysis of Control Structures for Reaction/Separation/Recycle Processes with Second-Order Reactions." <u>Ind. Eng. Chem. Res.</u> 35 (1996): 758-71.

Whitney, D. E. "Quasi-static assembly of compliantly supported rigid parts." <u>Journal of Dynamic Systems</u> 104 (1982): 65-77.

Wilkie, D. R. "Relation Between Force and Velocity in Human Muscle." <u>J. Physiol.</u> 110 (1950): 249-80.

Winters, Jack, and Lawrence Stark. "Analysis of Fundamental Human Movement Patterns Through the Use of In-Depth Antagonistic Muscle Models." <u>IEEE Transactions on Biomedical Engineering</u> 32 (1985): 826-39.

Wosch, Thomas, and Wendelin Feiten. "Reactive Motion Control for Human-Robot Tactile Interaction." IEEE, International Conference on Robotics & Automation, May 2002, Washington, DC. <u>Robotics & Automation 2002</u>. Vol. 4. IEEE, 2002. 3807-812.

Zabjek, K., and Et. Al. "Evaluation of segmental postural characteristics during quiet standing in control and Idiopathic Scoliosis patients." <u>Clinical Biomechanics</u> 20 (2005): 483-90.

Zhang, Li-Qun, and William Z. Rymer. "Simultaneous and Nonlinear Identification of Mechanical and Reflex Properties of Human Elbow Joint Muscles." <u>IEEE Transactions on Biomedical Engineering</u> 44 (1997): 1192-209.

Ziegler, J. G. "Optimum Settings for Automatic Controllers." <u>Transactions of the ASME</u> 115 (1993): 220-22.

STATIC TRIAL RAW DATA

Table A1-1: Averages of static trials for each model, per subject.

Subject	S1- RMS Displacement		S2- Peak Displacement		S3- Mean Operating Point	
	PD	BIO	PD	BIO	PD	BIO
1	0.149	0.189	0.078	0.258	91.288	89.435
2	0.264	0.208	0.329	0.314	87.299	87.239
3	0.301	0.356	0.499	0.577	91.822	91.726
4	0.181	0.245	0.317	0.128	94.641	94.786
5	0.088	0.219	0.164	0.268	90.405	89.865
6	0.064	0.059	0.051	0.139	87.132	87.227
7	0.068	0.160	0.126	0.222	92.176	90.677
8	0.126	0.089	0.103	0.180	93.523	93.949
9	0.107	0.362	0.226	0.297	93.178	93.007
10	0.286	0.595	0.484	0.874	88.868	89.223
11	0.135	0.145	0.171	0.190	88.060	86.848

Table A1-2: Detailed paired t-test results for (a) RMS displacement, (b) peak displacement, and (c) mean operating point.

a) RMS Displacement

	PD	*BIO*
Mean	0.161	0.239
Variance	0.007	0.023
t Stat	-2.248	
p-value	0.048*	
t Crit	2.228	

b) Peak Displacement

	PD	*BIO*
Mean	0.232	0.314
Variance	0.024	0.050
t Stat	-1.955	
p-value	0.079	
t Crit	2.228	

c) Mean Operating Point

	PD	*BIO*
Mean	90.763	90.362
Variance	6.809	7.574
t Stat	1.709	
p-value	0.118	
t Crit	2.228	

DYNAMIC TRIAL RAW DATA

Table A2-1: F-Test results for dynamic trials. Cells are grayscale-coded according to the model with the smallest variance; white when the human-like model is significantly less variant, black when the PD model is significantly less variant, and grey for insignificant differences in means.

f-test p values

Subject	Settling	Displacement	Error	St Error
1	0.148	0.230	0.394	0.339
2	0.088	0.451	0.067	0.119
3	0.028	0.208	0.444	0.052
4	0.004	0.444	0.102	0.156
5	0.067	0.082	0.400	0.438
6	0.001	0.082	0.026	0.258
7	0.511	0.420	0.477	0.075
8	1.02E-04	0.408	0.154	0.384
9	0.040	0.257	0.058	0.097
10	0.396	0.026	0.477	0.268
11	0.467	0.306	0.410	0.083
12	0.008	0.492	0.159	0.369
13	0.002	0.187	1.28E-04	0.267

Table A2-2: T-test results for dynamic performance criteria. Cells are grayscale-coded according to the model with the smallest variance; white when the human-like model is significantly less variant, black when the PD model is significantly less variant, and grey for insignificant differences in means.

t-test p values

Subject	Settling	Displacement	Error	St Error
1	1.62E-08	3.07E-08	0.720	0.705
2	0.406	1.31E-04	0.799	0.989
3	0.944	0.007	0.879	0.785
4	0.375	1.24E-08	0.680	0.003
5	0.028	2.31E-05	0.037	0.463
6	0.054	1.93E-09	0.133	0.999
7	0.237	4.81E-08	0.582	0.499
8	0.691	3.59E-08	0.001	0.452
9	0.723	0.001	0.122	0.204
10	0.370	4.16E-08	0.025	0.869
11	0.685	0.009	0.942	0.592
12	0.560	1.56E-05	0.776	0.310
13	0.716	4.55E-04	0.178	0.393

Table A2-3: Fisher's exact test distribution tables.

a) D1- Starting Error

	Pref	No Pref	Row
BIO	0	4	4
PID	1	8	9
Column	1	12	13
	p-crit:	0.692	
	Alt. p:	0.308	
	p:	0.308	

b) D2- Peak Displacement

	Pref	No Pref	Row
BIO	13	0	13
PID	0	0	0
Column	13	0	13
	p-crit:	1.000	
	Alt. p:	None	
	p:	0.00 (BIO)	

c) D3- Settling Time

	Pref	No Pref	Row
BIO	2	5	7
PID	0	6	6
Column	2	11	13
	p-crit:	0.269	
	Alt. p:	0.538, 0.192	
	p:	0.192	

d) D4- Settling Error

	Pref	No Pref	Row
BIO	1	2	3
PID	2	8	10
Column	3	10	13
	p-crit:	0.472	
	Alt. p:	0.420, 0.105, 0.003	
	p:	0.528	

Table A2-4: Coefficients of variation for dynamic criteria, listed by subject.

Subject	D1- Starting Error		D2- Peak Displacement		D3- Settling Time		D4- Settling Error	
	PD	BIO	PD	BIO	PD	BIO	PD	BIO
1	0.680	0.566	0.037	0.034	0.050	0.076	0.415	0.423
2	0.614	0.868	0.044	0.049	0.196	0.271	0.903	0.516
3	0.747	0.285	0.040	0.026	0.192	0.469	0.229	0.195
4	0.628	0.316	0.026	0.029	0.053	0.105	0.238	0.312
5	0.482	0.446	0.021	0.032	0.124	0.214	0.551	0.878
6	0.692	0.590	0.022	0.035	0.253	0.137	0.691	0.780
7	0.859	0.500	0.025	0.029	0.478	0.610	0.685	0.795
8	0.574	0.731	0.030	0.034	0.093	0.248	0.338	0.300
9	0.699	0.711	0.037	0.047	0.301	0.180	0.800	0.768
10	0.506	0.608	0.039	0.026	0.194	0.221	0.868	0.508
11	0.459	0.600	0.050	0.061	0.174	0.175	0.743	0.717
12	0.687	0.483	0.029	0.031	0.262	0.532	0.191	0.256
13	0.390	0.416	0.028	0.044	0.209	0.673	0.294	0.849

Table A2-5: Paired t-test analysis of coefficient of variation data for dynamic criteria. Starred results are significant.

7a) D1- Starting Error

	BIO	*PD*
Mean	0.547	0.616
Variance	0.027	0.017
t Stat	-1.147	
p value	**0.273**	
t Critical	2.178	

7b) D2- Peak Displacement

	BIO	*PD*
Mean	0.037	0.033
Variance	1.117E-4	8.16763E-05
t Stat	1.407	
p value	**0.185**	
t Critical	2.179	

7c) D3- Settling Time

	BIO	*PD*
Mean	0.301	0.198
Variance	0.040	0.013
t Stat	2.274	
p value	**0.042* (PD)**	
t Critical	2.179	

7d) D4- Settling Error

	BIO	*PD*
Mean	0.561	0.534
Variance	0.061	0.068
t Stat	0.398	
p value	**0.697**	
t Critical	2.179	